(19) Europäisches Patentamt
European Patent Office
Office européen des brevets

(11) **EP 1 906 821 B1**

(12) **EUROPEAN PATENT SPECIFICATION**

(45) Date of publication and mention of the grant of the patent:
15.01.2020 Bulletin 2020/03

(21) Application number: **06800185.8**

(22) Date of filing: **21.07.2006**

(51) Int Cl.:
A61B 5/0402 *(2006.01)* ***A61B 6/03*** *(2006.01)*
A61B 5/00 *(2006.01)* ***A61B 5/055*** *(2006.01)*
A61B 5/0408 *(2006.01)*

(86) International application number:
PCT/US2006/028287

(87) International publication number:
WO 2007/013994 (01.02.2007 Gazette 2007/05)

(54) **SYSTEM FOR NONINVASIVE ELECTROCARDIOGRAPHIC IMAGING (ECGI)**

SYSTEM FÜR NICHT-INVASIVE ELEKTROKARDIOGRAPHISCHE BILDGEBUNG (ECGI)

SYSTÈME D'IMAGERIE ELECTROCARDIOGRAPHIQUE NON INVASIVE (ECGI)

(84) Designated Contracting States:
AT BE BG CH CY CZ DE DK EE ES FI FR GB GR HU IE IS IT LI LT LU LV MC NL PL PT RO SE SI SK TR

(30) Priority: **22.07.2005 US 701626 P**

(43) Date of publication of application:
09.04.2008 Bulletin 2008/15

(60) Divisional application:
11010196.1 / 2 436 309

(73) Proprietor: **CASE WESTERN RESERVE UNIVERSITY**
Cleveland, Ohio 44106 (US)

(72) Inventors:
- **RUDY, Yoram**
  St. Louis, MO 63108 (US)
- **WANG, Yong**
  St. Louis, MO 63139 (US)
- **JIA, Ping**
  Solon, OH 44139 (US)

(74) Representative: **Gibbs, Richard et al**
Marks & Clerk LLP
Aurora
120 Bothwell Street
Glasgow G2 7JS (GB)

(56) References cited:
US-A- 5 146 926
US-A- 5 483 968
US-A- 6 047 206
US-A1- 2002 128 565
US-A1- 2003 120 163
US-B2- 6 772 004
US-B2- 6 856 830

- **Computer Methods and Programs in Biomedicine Elsevier Ireland, vol. 58, no. 2, 1999, pages 119-131, XP002556562 ISSN: 0169-2607**
- **SEGER M ET AL: "Lead field computation for the electrocardiographic inverse problem-finite elements versus boundary elements" COMPUTER METHODS AND PROGRAMS IN BIOMEDICINE, ELSEVIER, AMSTERDAM, NL, vol. 77, no. 3, 1 March 2005 (2005-03-01), pages 241-252, XP025296913 ISSN: 0169-2607 [retrieved on 2005-03-01]**
- **KARAGEORGHIS A ET AL: "The method of fundamental solutions for the numerical solution of the biharmonic equation" JOURNAL OF COMPUTATIONAL PHYSICS, LONDON, GB, vol. 69, no. 2, 1 April 1987 (1987-04-01), pages 434-459, XP024751894 ISSN: 0021-9991 [retrieved on 1987-04-01]**

EP 1 906 821 B1

Description

Statement Regarding Federally Sponsored Research or Development

[0001] This invention was made with government support under NIH-NHLBI Grant R37-HL-33343 awarded by the National Institutes of Health (NIH). The government may have certain rights in the invention

Field of the Invention

[0002] This invention relates to an improved technique for noninvasive electrocardiographic imaging (ECGI). In particular, the preferred embodiment of the present invention relates to a meshless noninvasive ECGI technique wherein a plurality of body surface potentials are noninvasively obtained and combined with data representing the geometry of a heart and body torso to generate electrocardiographic images that represent electrical activity of the heart.

Background of the Invention

[0003] Over 7 million people worldwide (around 400,000 in the U.S.) die annually from rhythm disorders of the heart. Many more people are disabled each year from such rhythm disorders. Despite these alarming statistics, the development of a noninvasive imaging modality for cardiac arrhythmias to help physicians identify patients at risk of sudden death, provide specific diagnoses, and guide therapy has only recently borne fruit.

[0004] Previous works by one of the inventors herein in the field of noninvasive ECGI are represented by U.S. Patent No. 6,772,004, entitled "System and Method for Non-Invasive Electrocardiographic Imaging" pending U.S. patent application 10/264,572, filed October 4, 2002, entitled "System and Methods for Noninvasive Electrocardiographic Imaging (ECGI) Using Generalized Minimum Residual (GMRES)" (published as U.S. published application 2003/0120163), and pending U.S. patent application 10/317,953, filed December 12, 2002, entitled "Systems and Methods for Determining a Surface Geometry" (published as U.S. published application 2004/0082870). These works disclose the computation of epicardial cardiac surface potentials, electrograms, and isochrones from noninvasively-measured body surface potentials using, in part, a technique known as the Boundary Element Method (BEM). For ease of reference, the technology disclosed in these applications will be referred to as BEM ECGI hereinafter. With BEM ECGI, 3D surface meshes of a patient's torso surface and epicardial cardiac surface are created to compute a matrix of coefficients A for translating measured body surface potentials to epicardial cardiac surface potentials (which in turn can be translated into electrograms and/or isochrones). This 3D surface meshing is an iterative time-consuming task that requires large memory resources, The BEM ECGI process is further slowed by the manual optimization of the surface meshes that is generally required to maintain accuracy in reconstructing the epicardial cardiac surface potentials. Meshing generally involves the definition of triangular- shaped elements (or elements of other shapes) that together define a 3D boundary around a surface of interest. Software can be used to initially automatically create the 3D surface mesh. However, this initial mesh will often need to be optimized to improve its accuracy, thereby further adding to the time required to accurately reconstruct the surface potentials and, in turn, further detracting from BEM ECGI' s applicability to clinical applications. Moreover, the skill level required to optimize body surface and heart surface meshes is generally high, which limits the pool of people who are qualified to conduct BEM ECGI. Further still, even with a skilled person performing mesh optimization, it is believed by the inventors herein that BEM meshes nevertheless exhibit difficulty in accommodating complex heart geometries (particularly concave geometries) such as those that may be found in patients suffering from heart disease.

[0005] Publication No XP002556562 (Computer Methods and Programs in Biomedicine, vol 58 (1999) 119 - 131, FISCHER et al) discloses a method in which eight-noded quadrilateral boundry elements are applied to the electrocardiographic inverse problem as an example for high-order boundry elements.

[0006] Publication No XP025296913 (Computer Methods and Programs in Biomedicine, vol 77 (2005) 242 - 252, SEGER et al) discloses a comparison of two methods applied for computing the lead field matrix which is calculated to solve the inverse problem of electrocardiology, namely the Boundry Element Method (BEM) and the Finite element Method (FEM).

Summary

[0007] According to an aspect of the present invention, there is provided a non-invasive system for determining electrical activity for a heart of a living being according to the appended claims.

[0008] The inventors herein have developed an ECGI system that employs a meshless algorithm to reconstruct heart surface electrical potentials from noninvasively measured body surface electrical potentials and data describing the geometrical relationship between the locations where the body surface potentials were measured and the heart surface. This meshless algorithm operates to translate electrical potentials measured at a plurality of locations along a body

surface to any surface of interest that is defined between the epicardial cardiac surface and the body surface. Preferably, the surface of interest to which the body surface electrical potentials are translated is the epicardial cardiac surface. However, as an example not belonging to the invention, a practitioner may choose to translate the body surface electrical potentials to any arbitrary surface between the epicardial cardiac surface and the body surface. Accordingly, the term "epicardial envelope" as used herein refers to any surface on or outside the epicardial cardiac surface and inside the volume defined by the body surface that at least partially encloses the epicardial cardiac surface. While the term "epicardial envelope" encompasses the actual outer surface of the epicardium, the term "epicardial cardiac surface" as used herein refers specifically to the actual outer surface of the epicardium.

[0009] In the most preferred embodiment, this meshless algorithm is the method of fundamental solution (MFS). As such, the preferred embodiment of the present invention will often be referred to herein as MFS ECGI.

[0010] Rather than employing a surface mesh of the body surface and heart surface, MFS ECGI operates to define a plurality of virtual source nodes both outside the body surface and inside the heart surface. The virtual source nodes that are located outside the body surface define a surface boundary outside the body surface. The virtual source nodes that are located inside the heart surface define a surface boundary inside the heart surface. Based on the known geometrical relationships between the virtual source nodes, the electrode positions where the body surface potentials are measured, and the epicardial nodes for which the heart surface electrical potentials are computed, the MFS technique can readily reconstruct the epicardial cardiac surface potentials from the measured body surface potentials.

[0011] Experimentation has shown that this MFS ECGI technique operates at speeds that are of orders of magnitude faster than BEM ECGI, all while consuming less memory resources and being amenable to implementation via relatively short software code. Further still, the inventors herein believe that this increase in speed and efficiency has not hindered accuracy. In fact, experimentation has shown that MFS ECGI is at least as accurate as and in some cases of higher accuracy than BEM ECGI.

[0012] The inventors herein believe that the improved performance of MFS ECGI relative to BEM ECGI opens wide new windows of opportunity for noninvasive ECGI, particularly in connection with medical applications where time is of the essence such as interventional medical applications (including but not limited to ablation of arrhythmia substrates, targeted drug delivery, lead placement for implanted devices such as pacemakers and implanted cardioverters/defibrillators (ICDs), and other surgical procedures), guidance of interventional medical applications, evaluation of drug effect, risk stratification, and exercise stress tests. Even in less time critical applications, the inventors herein believe that the present invention will dramatically improve turnaround time for ECGI such that results can be obtained in minutes rather than hours, even while the patient remains in the cardiac electrophysiology laboratory, thereby allowing for rapid diagnosis and possible ECGI-guided intervention.

[0013] Moreover, because of the reduced complexity and increased automation of MFS ECGI relative to BEM ECGI, it is believed by the inventors herein that the amount of training required by a user (such as a physician, fellow, or medical assistant) can be greatly reduced, thereby allowing for wider use in the field

[0014] These and other features and advantages of the present invention are set forth below and in the enclosed figures.

Brief Description of the Drawings

[0015]

Figure 1 illustrates a block diagram overview of a preferred system for meshless noninvasive ECGI;
Figures 2(a) and 2(b) depict exemplary geometry determining devices;
Figure 3 depicts an exemplary high level flowchart for performing noninvasive ECGI;
Figure 4 is an exemplary flowchart for performing meshless noninvasive ECGI;
Figures 5(a)-(e) depict how source nodes can be configured during the preferred meshless noninvasive ECGI process;
Figure 6 depicts the matrix equation for relating torso surface potentials to source nodes;
Figure 7 depicts the matrix equation for relating source nodes to epicardial cardiac surface potentials;
Figure 8 is a chart comparing computation times for MFS ECGI versus BEM ECGI;
Figure 9 depicts heart surface potential maps for directly-measured heart surface potentials, heart surface potentials reconstructed using MFS ECGI, and heart surface potentials reconstructed using BEM ECGI;
Figure 10 depicts heart surface electrograms (both measured and reconstructed via MFS ECGI) from various locations on the heart surface for pacing from a single site;
Figure 11 depicts heart surface isochrone maps for pacing from a single site; both for measured potentials and for potentials reconstructed via MFS ECGI;
Figure 12 depicts reconstruction results for a right ventricular epicardial pacing site in a human subject using both BEM ECGI and MFS ECGI, wherein the MFS ECGI reconstruction is shown to avoid mesh-related artifacts;
Figure 13 depicts human heart surface isochrone maps and potential maps, using MFS ECGI, for pacing from both

a right ventricle (RV) site and a left ventricle (LV) site; and

Figure 14 depicts normal atrial activation isochrones, derived from potentials reconstructed via MFS ECGI.

Detailed Description of the Preferred Embodiment

[0016] Figure 1 depicts a block diagram overview of a preferred system 100 for performing meshless noninvasive ECGI. The system 100 preferably comprises a plurality of electrodes 104 (mounted on strips 102, a vest, or in some other array) in communication with a signal acquisition and processing device 106. The electrodes 104 serve to sense a plurality of electrical potentials on a patient's body surface. The signal acquisition and processing device 106 operates to process this sensed data to a form suitable for digital processing, as is known in the art. The system 100 also comprises a geometry determining device 116 that serves to generate data that is indicative of the geometrical relationship between the electrodes 104 and one or more points of interest within the patient (e.g., the patient's epicardial cardiac surface).

[0017] Processor 114 operates to (1) receive data from both the electrodes 104 (by way of the signal acquisition and processing device 106) and the geometry determining device 116 and (2) reconstruct epicardial cardiac surface potentials from the received data. The reconstructed epicardial potentials can then be used to provide, via the output device 118, electrograms, isochrones (activation maps), epicardial cardiac potential maps, or other data representations derived from the epicardial potentials (e.g., integral maps, recovery maps, activation-recovery interval maps, etc.). An example of a suitable processor 114 for the present invention is a conventional desktop or laptop computer, such as a 2.4 GHz laptop computer with a gigabyte of RAM. However, as would be understood by those having ordinary skill in the art, any processor with sufficient memory resources and computational speed would be suitable for use as processor 114. Output device 118 may be any device capable of effectively communicating the results of the reconstruction to a user, such as a display monitor and/or printer associated with the processor 114, as would be understood by those having ordinary skill in the art.

[0018] It is also worth noting that a variety of known techniques for electronic data communication can be used as the data links between the various elements depicted in Figure 1, as would be understood by those of ordinary skill in the art. Furthermore, it should be understood that the meshless ECGI technique described herein can readily be implemented in software and/or hardware for execution by one or more processors to compute epicardial cardiac surface potentials. Moreover, in some instances the processor 114 and geometry determining device may be integrated into the same platform, such as a CT scanner, an MRI scanner, a bi-plane X-ray fluoroscopy apparatus, or an ultrasound echocardiography apparatus that has MFS ECGI processing capabilities built-in.

[0019] Electrodes 104 are preferably arranged on a plurality of strips 102 that can be placed in position on the torso of a patient undergoing ECGI. Alternatively, a vest arrangement as shown in U.S. patent 6,772,004 and pending U.S. patent application 10/264,572 may also be used. As mentioned above, electrodes 104 measure the electrical potentials on the patient's torso. The electrodes 104 that are used are preferably electrodes that are visible in the imaging modality used by the geometry determining device 116. Otherwise, it is preferred that appropriate markers be placed on the electrodes to render them visible in the images produced by the geometry determining device 116. When practicing the present invention, the total number of electrodes 104, the number of electrodes 104 per strip 102, the number of electrode strips 102, and the placement of the electrode strips 102 on the patient can be variable according to the needs of a practitioner of the present invention. However, it is preferred that as much of the patient's torso (front, back, and sides) be covered by electrodes 104 as possible. For example, the total number N of electrodes 104 could range from 120 to 250. However, the value of N may be more or less than a value within this range, as would be understood by a person having ordinary skill in the art. However, the inventors herein believe that the use of too few electrodes will reduce the accuracy of the reconstructed epicardial cardiac surface potentials.

[0020] The electrodes can be wet electrodes or dry electrodes, as would be understood by those having ordinary skill in the art. By avoiding the use of gels, short circuiting risks arising from a high concentration of electrodes can be reduced. An example of a suitable type of electrode to obtain body surface potentials is a silver/silver chloride (Ag/AgCl) electrode. However, other types of electrodes such as carbon electrodes can also be used. However, if CT is used as the imaging modality for the geometry determining device, then it is preferred that CT markers be disposed on the carbon electrodes to render them visible in the CT images.

[0021] The signal acquisition and processing device 106 is preferably a multichannel device that operates to receive the sensed electrical potentials from the electrodes 104, process that data, and supply it to processor 114. Practitioners of the present invention may select a commercially-available system to use as the signal acquisition and processing device 106. For example, the Active Two system that is available from BioSemi of WG-Plein 129, 10545C, Amsterdam, Netherlands, which is a 256-channel, DC amplifier, 24 bit resolution biopotential measurement system, may serve as device 106. The Active Two biopotential measurement system includes an analog-to-digital converter (ADC) that receives electrode data from electrodes 104, a power source (battery and charger), a USB2 receiver that receives the digital output from the ADC via a fiber optic connection and provides the digital electrode data to acquisition software resident on processor 114 via a USB2 connection. The analog input box that is also part of the Active Two system may be omitted

from the practice of the preferred embodiment.

[0022] It should also be noted that custom-designed signal acquisition and processing device 106 can also be used, such as the one described in prior U.S. patent 6,772,004 and pending U.S. patent application 10/264,572.

[0023] The geometry determining device 116 may take a variety of forms, as described in prior U.S. patent 6,772,004 and pending U.S. patent applications 10/264,572 and 10/317,953, including x-ray, ultrasound, computed tomography (CT) and magnetic resonance imaging (MRI). For example, as shown in Figure 2(a), the geometry determining device 116 may take the form of a CT scanner or MRI device 200. The operation and collection of data therefrom will be apparent to those of ordinary skill in the art. In one embodiment, the CT scanner/MRI device 200 is used to generate data, or images, to determine torso geometry and, consequently, body surface electrode positions as well as an epicardial envelope surrounding the heart. As those of skill in the art will appreciate, the epicardial envelope is a suitable estimate of the epicardial cardiac surface itself, which could also be determined. It should also be recognized that locating the epicardial envelope or surface necessarily involves location of the heart. As a further example, as shown in Figure 2(b) and described in greater detail in prior U.S. patent 6,772,004 and pending U.S. patent applications 10/264,572 and 10/317,953, the geometry determining device 116 may also take the form of a bi-plane x-ray machine 202 and a digitizer 204.

[0024] Figure 3 depicts a high level view of the noninvasive ECGI process. After appropriately applying electrode strips 102 (or vest) to the patient's torso and after appropriately setting up a geometry determining device 116 such as a CT scanner (step a), (1) a plurality of ECG potentials on the patient's torso can be measured via the electrodes (step d), (2) these measured ECG potentials can be processed to generate body surface potential data (step e), (3) a plurality of transverse CT images of the patient's torso can be obtained, and (4) these CT images can be processed to determine the patient's 3D heart-torso geometry (step c). At step f, the software components of the preferred embodiment preferably operate to combine and process the body surface potential data and the heart-torso geometry data to reconstruct estimates of the epicardial cardiac surface potentials. These reconstructed epicardial cardiac surface potentials can in turn be processed at step g to generate appropriate epicardial cardiac surface potential maps, epicardial cardiac surface electrograms, and epicardial cardiac surface isochrones.

[0025] Figure 4 depicts the preferred flow for the meshless noninvasive ECGI of the present invention in greater detail. Signal acquisition and processing as described in connection with device 106 is performed on the sensed body surface potential data 400 from electrodes 104 to generate a 1xN vector V_T of torso surface potentials, wherein N preferably represents the total number of electrodes 104 used by system 100 such that $V_T(i)$ represents the torso surface potential that was measured by a particular electrode 104(i). V_T serves as a body surface potential map (BPSM). It is desired to reconstruct an epicardial cardiac surface potential map V_E from V_T using geometry data 402 that identifies the geometrical relationship between the torso surface, torso electrodes, and epicardial cardiac surface. This geometry data can be obtained from geometry determining device 116 as described in connection with Figures 1 and 2. It should be recognized that in a clinical setting, the geometry data 402 would be generated by the geometry determining device 116; however, it should also be noted that when executing the MFS ECGI technique for testing and/or validation purposes, the geometry data 402 may be known parameters, such as those associated with geometric spheres and torso tanks (used in testing), that are simply input to the system.

[0026] Returning to a clinical example, the geometry data can be a plurality of CT slices from which the patient's torso surface, the torso electrodes disposed on the patient's torso surface, and epicardial cardiac surface can be identified. Furthermore, based on the known slice thickness and scan parameters, the location of any given point on each slice can be determined in a three-dimensional (3D) coordinate space, and thus the geometrical relationship between any two points can also be determined in the 3D coordinate space.

[0027] Figure 5(a) depicts an exemplary CT scan in which the patient's torso surface 500 and epicardial cardiac surface 502 are visible. For the purposes of explaining the meshless technique referred to herein as the Method of Fundamental Solution (MFS), a two-dimensional (2D) example will be given. However, it should be understood by those having ordinary skill in the art that the MFS technique can be readily extended to three dimensions for use in real world applications. Further, it should be understood that the surfaces and node locations depicted in Figures 5(a)-(e) are exemplary only and are not drawn to scale.

[0028] Visible in the image of Figure 5(a) are N torso electrodes (or torso nodes) TN_1 through TN_N. As can be seen from Figure 5(a), in this example, N equals 8. However, it should be understood this value of N is exemplary only and chosen for simplicity in connection with explaining the principles of the preferred embodiment of the present invention. As previously explained, in practice, it is preferred that much larger values of N be used.

[0029] Each torso node TN_i corresponds to the location where an electrical potential of the patient's torso surface 500 has been measured. The goal of the preferred embodiment is to translate the potential measurements at the torso nodes to nodes located on the epicardial envelope. In a most preferred embodiment, the torso node measurements are translated to nodes on the epicardial cardiac surface 502. To perform this translation to the epicardial cardiac surface, the locations of the nodes on the epicardial cardiac surface 502 (referred to herein as "epicardial nodes" - wherein "epicardial nodes" refers to the nodes that are defined on the epicardial cardiac surface specifically or on the epicardial envelope) should

first be determined.

[0030] As part of this process, Figure 5(b) depicts a plurality of epicardial nodes that are located on the patient's epicardial cardiac surface 502. If the torso node measurements are being translated to nodes on the epicardial envelope other than the epicardial cardiac surface 502, then the epicardial nodes will be located on the particular surface of interest. Because the heart is clearly visible in the CT slices, any of a variety of techniques can be used to identify the epicardial cardiac surface 502. For example, commercially-available or custom-designed medical image visualization and segmentation software, such as the well-known Amira 3D visualization software package, can be used to identify, segment, and label the heart and heart surface 502 in the CT slices. Segmentation can be performed manually or automatically by known algorithms in the art. To appropriately place each epicardial node (EN), either a manual or automatic technique can be used to place a plurality M of ENs on the epicardial cardiac surface 502. With a manual technique, a user manually places the ENs at user-selected points along the epicardial cardiac surface 502. With an automated technique, an algorithm automatically distributes the ENs along the epicardial cardiac surface 502. It is worth noting that accuracy in node placement is important because any error in determining node position can cause computational error during the inverse computation described below. The value of M can vary as a design choice by a practitioner of the present invention. However, it is preferred that a sufficient number of ENs be placed on surface 502 such that the MFS technique described herein exhibits a desired degree of resolution. An example of a suitable value for M is 100 or more. Preferably, these M ENs are evenly distributed over the epicardial cardiac surface 502, but this need not be the case. For example, in some instances it may be desirable to obtain high spatial resolution reconstruction in a certain area of the heart, in which case a practitioner of the present invention may choose to concentrate more ENs in that area than in other areas.

[0031] Next, at step 406, a plurality of source nodes are configured. These source nodes are "virtual" nodes that are placed to define two surfaces - one that is outside the torso surface 500 and one that is inside the epicardial cardiac surface 502. The shape of each of these surfaces can be arbitrary so long as the outer surface remains outside the torso surface 500 and the inner surface remains inside the epicardial cardiac surface 502. Two general approaches may be used when configuring the source nodes: (1) a static configuration where the source nodes that define the fictitious boundaries are placed at fixed and pre-selected locations, and (2) a dynamic configuration where the locations of the source nodes that define the fictitious boundaries are determined dynamically by a complex nonlinear optimization procedure. Because of the complex and time-consuming nature of the nonlinear optimization procedure, dynamic configuration of source nodes is not preferred. Instead, it is preferred that a static configuration be used.

[0032] With a static configuration of source nodes, several configuration options are available when practicing the present invention, as would be understood by those having ordinary skill in the art. A preferred static configuration technique is a technique wherein the source nodes are placed at locations parallel to the torso surface (some distance outward therefrom) and epicardial cardiac surface (some distance inward therefrom). With this technique, the source nodes are defined such that (1) the outer surface source nodes are placed some fixed distance outward from each torso node along the rays extending from C_0 through each of the torso nodes, and (2) the inner surface source nodes are placed some fixed distance inward from each epicardial node along the rays extending from C_0 through each of the epicardial nodes, wherein C_0 represents the geometric center of the heart. C_0 can be readily determined by conventional segmentation software as previously described. The fixed distance that is used for source node placement can be variable as a design choice for a practitioner of the present invention. However, in one embodiment, a ratio of 1.2:1 can be used for configuring source nodes from the torso nodes and a ratio of 0.8:1 can be used for configuring source nodes for the epicardial nodes. In this example (wherein each source node that defines the fictitious surface outside the torso surface is inflated at a 1.2:1 ratio), if a given torso node was located 1 unit of measurement from C_0, then the source node corresponding to that torso node would be located along a ray extending from C_0 through that torso node at a location 1.2 units of measurement from C_0. Also with this example (wherein each source node that defines the fictitious surface inside the epicardial cardiac surface is deflated at a 0.8:1 ratio), if a given epicardial node was located 1 unit of measurement from C_0, then the source node corresponding to that epicardial node would be located along a ray extending from C_0 through that epicardial node at a location 0.8 units of measurement from C_0.

[0033] Figure 5(c) depicts such a placement of source nodes SN_1 through SN_{24}. Continuing from the examples of Figures 5(a) and (b), wherein N TNs and M ENs have been defined, it can be seen that the total number P of source nodes will be N+M in the preferred embodiment. For this example, where N equals 8 and M equals 16, this means that P equals 24. However, this need not be the case, as the number of source nodes can be selected independently of the number of torso nodes and epicardial nodes. Source nodes SN_1 through SN_8 define an outer surface wherein SN_1 is some fixed distance outward from TN_1 along a ray extending from C_0 through TN_1, wherein SN_2 is that fixed distance outward from TN_2 along a ray extending from C_0 through TN_2, and so on. Source nodes SN_9 through SN_{24} define an inner surface wherein SN_9 is some fixed distance inward from EN_1 along a ray extending from C_0 through EN_1, wherein SN_{10} is that fixed distance inward from EN_2 along a ray extending from C_0 through EN_{10}, and so on. Furthermore, as would be understood by those having ordinary skill in the art, the coordinate values of each source node SN_i in the 3D coordinate space of the patient's torso are known, thereby making distance determinations between (1) each source

node and each torso node and (2) each source node and each epicardial node easy to calculate.

[0034] At step 408, the process operates to determine a transfer matrix A that translates the measured torso potentials V_T at each torso node to a plurality of source node coefficients, which reflect the "strength" of each source node, such that:

$$V_T = A\Gamma$$

wherein A is a 2NxP+1 matrix, wherein N represents the total number of torso nodes and wherein P represents the total number of source nodes. This equation is shown in greater detail in Figure 6, wherein the vector V_T is represented by the torso surface potentials at the various torso nodes for $V_T(1)$ through $V_T(N)$ and 0 (to represent the current) for $V_T(N+1)$ through $V_T(2N)$. The value of each entry $a_{j,k}$ in matrix A is a function of the distance between torso node TN_j and source node SN_k., preferably such that:

$$a_{j,k} = \frac{1}{r_{j,k}}$$

wherein $r_{j,k}$ equals the distance between torso node TN_j and source node SN_k. Figure 5(d) depicts various distances r from torso node TN_1 to exemplary source nodes (in this example, SN_1, SN_2, and SNio). For ease of reference, Figure 5(d) does not depict each distance r from each torso node to each source node, but a person having ordinary skill in the art would readily understand from Figure 5(d) how each value of r would be determined.

[0035] The values $d(a_{j,k})/dn$ in matrix A represent the derivatives of each $a_{j,k}$ term relative to the normal n defined by the torso surface 500 at the applicable torso node. Figure 5(e) illustrates the relationship between $r_{j,k}$ and normal n for an exemplary torso node TN(x). The normal to the torso surface 500 at given torso node TN(x) is defined as the perpendicular to the torso surface tangent at that torso node TN(x). Thus, the $d(a_{x,k})/dn$ terms for the row in A corresponding to torso node TN(x) will be computed from the normal to the torso surface 500 at TN(x), as shown in Figure 5(e).

[0036] Because each value for $r_{j,k}$ is readily calculable in view of the known coordinates of each torso node and each source node, the entries in matrix A are all known. Also, V_T is known as its values are measured by the torso electrodes (and the zero terms for the current entries in the vector). Therefore, the 1xP+1 vector Γ is the only unknown. To find each value γ_i in Γ, the inverse of A needs to be calculated at step 410, and wherein:

$$\Gamma = A^{-1}V_T$$

[0037] The computation of Γ is an ill-posed problem as small perturbations in the data (e.g., potential measurement noise and/or geometrical inaccuracy) can cause large unbounded errors. To reduce these potential errors, a variety of mathematical schemes that are known in the art can be used. Two schemes that are believed to provide effective results are Tikhonov zero order regularization and the Generalized Minimal Residual (GMRes) method. These techniques are described in U.S. Patent No. 6,772,004 and pending U.S. patent application 10/264,572. By following the teachings of these references (wherein the variable V_E as described in those references in connection with Tikhonov regularization and GMRes is replaced by Γ), a person having ordinary skill in the art can readily perform the inverse computation of step 410 to determine Γ (represented as source node coefficients 412 (γ_0 through γ_P) in Figure 4).

[0038] Once Γ is known, a forward computation 416 can be used to determine the epicardial cardiac surface potentials V_E. To do so, at step 414, a transfer matrix B must first be computed. Matrix B operates to translate the source node coefficients γ_0 through γ_P to epicardial cardiac surface potentials at each epicardial node EN_1 through EN_M such that:

$$V_E = B\Gamma$$

wherein B is a MxP+1 matrix, wherein M represents the total number of epicardial nodes and wherein P represents the total number of source nodes. This equation is shown in greater detail in Figure 7 which continues the example set forth in Figures 5 and 6. The value of each entry $b_{j,k}$ in matrix B is a function of the distance between epicardial node EN_j and source node SN_k, preferably such that:

$$b_{j,k} = \frac{1}{r_{j,k}}$$

wherein $r_{j,k}$ equals the distance between epicardial node EN_j and source node SN_k, which is the same principle shown in Figure 5(d) albeit using epicardial nodes rather than torso nodes. As each value for $r_{j,k}$ is readily calculable, the entries in matrix B are all known, which allows for a straightforward calculation of V_E from B and Γ.

[0039] Each entry $V_E(EN_i)$ within V_E will represent an estimation of the epicardial cardiac surface potential at the location on the epicardium defined by EN_i. From V_E (or from a plurality of V_E's calculated from a plurality of successively measured V_T's, as may be appropriate), persons having ordinary skill in the art can readily produce a variety of potential maps, electrograms, isochrone maps, recovery maps, integral maps, and activation-recovery interval maps of the patient's epicardial cardiac surface at step 418. As can be seen from the foregoing description, V_E can be computed from V_T without requiring a mesh of the torso or heart surfaces, thereby (among other advantages) greatly improving the speed of calculation for V_E. Additional details about the MFS technique are included herewith in Appendix A.

Experimental Results - Computational Speed:

[0040] The reconstructed epicardial cardiac surface potentials V_E were verified using benchmark data derived from a human-shaped torso-tank, the details of which are described in U.S. patent 6,772,004. Additionally, data from experimentation using the torso tank allowed for comparisons to be made between the ECGI technique using MFS, the ECGI technique using BEM, and directly measured epicardial potentials.

[0041] With respect to computation time, experimentation has shown that, using a laptop computer with a Pentium Mobile 1.7 GHz processor and 1G of RAM, BEM ECGI takes approximately 50.5 seconds to construct its transfer matrix A and achieve epicardial cardiac surface potential reconstruction for one time frame, while MFS ECGI in accordance with the teachings herein only takes about 0.2 seconds to form its transfer matrices A and B and achieve epicardial cardiac surface potential reconstruction for one time frame. The marked advantage in computation speed enjoyed by the MFS technique of the present invention over the prior BEM technique is shown in Figure 8. Moreover, it is worth noting that this computation time comparison did not take into account the additional manual editing time that the prior BEM ECGI technique requires when the user optimizes the torso and heart meshes. As such, the meshless technique of the present invention is expected to exhibit an even greater computation time advantage over the BEM ECGI technique than that depicted in Figure 8.

[0042] Further still, it is worth noting that in the comparison shown in Figure 8, abundant RAM (1G) was provided. It can be expected that in real world clinical applications, the RAM will be shared with other programs on the same machine, in which case less RAM will be available to the ECGI process. Because the BEM ECGI technique consumes significantly more RAM resources than does the meshless ECGI technique (it is believed that the MFS technique's elimination of the need to generate and manipulate 3D surface meshes of the heart and torso may possibly provide at least 66% savings in consumed RAM resources), it is believed that the MFS ECGI technique can operate at high speeds (relative to BEM ECGI) even in the face of reduced RAM.

Experimental Results - Single Pacing:

[0043] Focal sites of initiation of arrhythmogenic activity can result from abnormal automaticity, triggered activity, or micro-reentry. Because the focus is usually confined to a small region of the myocardium, it can be simulated by pacing the myocardium at a single site. Locating the ectopic focus is important for activities such as diagnosis and guiding an interventional therapeutic procedure (e.g., ablation).

[0044] Figure 9 shows electric potential maps 25 ms after pacing from a single site; the pacing site being marked by an asterisk. The top row of Figure 9 shows directly (i.e., invasively) measured heart surface potentials. The middle row shows heart surface potentials that were reconstructed using the MFS ECGI technique of the present invention. The bottom row shows heart surface potentials that were reconstructed using the prior BEM ECGI technique. The pacing site reconstructed by MFS ECGI is located only about 4 mm from its measured location, at the center of the potential minimum (blue). As can be seen, the potentials reconstructed via MFS ECGI show a high level of correspondence with the directly measured potentials. The pacing site reconstructed by BEM ECGI is located about 6 mm from its measured location. Additional examples of the improved accuracy of MFS ECGI relative to BEM ECGI are shown in Figure 9 via the higher correlation coefficient (CC) score and the lower relative error (RE) score. Moreover, not only do these results show that MFS ECGI is more accurate than BEM ECGI, but these results further confirm that MFS ECGI is considerably faster than BEM ECGI - the computation time per frame (CT) for MFS ECGI in this experiment is shown to be 0.2 seconds (versus 52 seconds for BEM ECGI). Appendix B describes how these CC and RE values were computed.

[0045] As is known in the art, electrograms can be formed from heart surface potential maps by developing such maps over successive time frames and then organizing the time series of maps by epicardial location. Figures 10(A)-(D) show various electrograms derived in this manner. Figure 10(A) shows four views of the epicardial cardiac surface. The numbers 1-9 in the boxes shown in Figure 10(A) identify the locations of nine electrodes whose measured electrograms and MFS ECGI-reconstructed electrograms are displayed in Figures 10(B)-(D). Sites 1-3 are relatively close to the pacing

site; sites 4-6 are relatively away from the pacing site; and sites 7-9 are relatively far away from the pacing site.

[0046] Figure 10(B) depicts the monophasic negative (Q wave) electrograms from sites 1, 2 and 3 from both direct measurements and MFS ECGI reconstruction. Figure 10(C) depicts the biphasic electrograms from sites 4, 5, and 6 from both direct measurements and MFS ECGI reconstruction. Figure 10(D) depicts the monophasic positive (R wave) electrograms from sites 7, 8, and 9 from both direct measurements and MFS ECGI reconstruction. The displayed CC value in each MFS ECGI electrogram indicates the level of similarity between the MFS ECGI reconstructed electrograms and the directly measured electrograms. As can be seen, there is a high degree of correlation between the two.

[0047] As is known in the art, isochrones for either measured or reconstructed epicardial cardiac surface potential data can be computed by taking the time of the epicardial activity at a given location as the time of maximum negative dV/dt of the temporal electrogram (which can be referred to as "intrinsic deflection") at that location. Isochrones provide a faithful and direct depiction of the epicardial activation sequence, which includes potential spatial non-uniformities of activation spread (e.g., regions of sparse or crowded isochrones depicting fast or slow speed respectively). Figure 11 provides a comparison of heart surface isochrone maps developed from measured potentials (the top row of Figure 11) and heart surface isochrone maps developed from potentials that have been reconstructed using MFS ECGI. As can be seen, the regions of earliest activation (shown in dark blue) are reproduced accurately in the MFS ECGI computed isochrone maps, as is the entire sequence of epicardial activation.

[0048] The development of optimal 3D surface meshes for the heart and torso geometry that is required by BEM ECGI is a difficult task. Non-optimal meshing will often introduce mesh-related artifacts in the BEM ECGI reconstructions, thereby decreasing the accuracy of BEM ECGI and hindering a physician's ability ECGI-reconstructed electrograms are displayed in Figures 10(B)-(D). Sites 1-3 are relatively close to the pacing site; sites 4-6 are relatively away from the pacing site; and sites 7-9 are relatively far away from the pacing site.

[0049] Figure 10(B) depicts the monophasic negative (Q wave) electrograms from sites 1, 2 and 3 from both direct measurements and MFS ECGI reconstruction. Figure 10(C) depicts the biphasic electrograms from sites 4, 5, and 6 from both direct measurements and MFS ECGI reconstruction. Figure 10(D) depicts the monophasic positive (R wave) electrograms from sites 7, 8, and 9 from both direct measurements and MFS ECGI reconstruction. The displayed CC value in each MFS ECGI electrogram indicates the level of similarity between the MFS ECGI reconstructed electrograms and the directly measured electrograms. As can be seen, there is a high degree of correlation between the two.

[0050] As is known in the art, isochrones for either measured or reconstructed epicardial cardiac surface potential data can be computed by taking the time of the epicardial activity at a given location as the time of maximum negative dV/dt of the temporal electrogram (which can be referred to as "intrinsic deflection") at that location. Isochrones provide a faithful and direct depiction of the epicardial activation sequence, which includes potential spatial non-uniformities of activation spread (e.g., regions of sparse or crowded isochrones depicting fast or slow speed respectively). Figure 11 provides a comparison of heart surface isochrone maps developed from measured potentials (the top row of Figure 11) and heart surface isochrone maps developed from potentials that have been reconstructed using MFS ECGI. As can be seen, the regions of earliest activation (shown in dark blue) are reproduced accurately in the MFS ECGI computed isochrone maps, as is the entire sequence of epicardial activation.

[0051] The development of optimal 3D surface meshes for the heart and torso geometry that is required by BEM ECGI is a difficult task. Non-optimal meshing will often introduce mesh-related artifacts in the BEM ECGI reconstructions, thereby decreasing the accuracy of BEM ECGI and hindering a physician's ability to interpret the reconstruction results. However, because MFS ECGI does not utilize a mesh to reconstruct epicardial cardiac surface potentials, it naturally avoids these mesh-related artifacts, which is a significant improvement over BEM ECGI. Panel A of Figure 12 depicts heart surface potential maps 25 ms after right ventricular pacing from a single site (indicated by the white asterisk) in a human subject using both BEM ECGI and MFS ECGI, wherein the MFS ECGI reconstruction is shown to avoid mesh-related artifacts (the fragmentation of the minimum blue shown in the BEM ECGI panel). Panel B depicts these maps during repolarization. Avoidance of the mesh-related artifacts allows the pacing site to be more accurately located; wherein the error in locating the pacing site was 14 mm using BEM ECGI versus 7 mm using MFS ECGI.

Experimental Results - Human Biventricular Pacing:

[0052] Another area where MFS ECGI shows great promise is the investigation of heart activity patterns in cardiac resynchronization therapy (CRT) patients. CRT was recently introduced for chronic heart failure patients. However, the availability of information on both the electrical and mechanical behavior of the heart during CRT has been extremely limited because of previous inabilities to noninvasively map heart activity. However, with the development of MFS ECGI, an excellent tool is provided for investigating the heart activity patterns in CRT patients. Figure 13 depicts human heart surface isochrone maps and potential maps, using MFS ECGI, for pacing from both a right ventricle (RV) site and a left ventricle (LV) (indicated by the asterisks). Figure 13 demonstrates that in a CRT study, both LV and RV pacing sites can be accurately located using MFS ECGI. Experiments have shown that, with MFS ECGI, the location errors for the RV pacing site and the LV pacing site are 5.2 mm and 7.4 mm respectively.

Experimental Results - Human Normal Atria Activation:

[0053] As discussed above, the geometry of human atria are sufficiently complex that mesh-based methods such as BEM require significant time, human intervention, and computational resources to obtain an accurate 3D surface mesh. However, as mentioned above, MFS ECGI eliminates this meshing requirement and allows for faster and more accurate potential reconstructions. This is believed to be particularly true for complex atria geometry. Figure 14 shows the normal atrial activation isochrones computed using MFS ECGI reconstructed potentials for a healthy volunteer. As can be seen, earliest activation starts in the right atrium (RA), near the anatomical location of the sinoatrial node (SA node). From the SA node, the impulse propagates to the left atrium (LA) and the rest of the RA. The LA appendage (LAA) is activated last. The abbreviation SVC in Figure 14 refers to the superior vena cava and the abbreviation PV refers to the pulmonary veins. The inventors herein believe that the noninvasively reconstructed atrial isochrone produced by MFS ECGI is highly consistent with the invasive measurements as described in Durrer D. et al., Total excitation of the isolated human heart, Circulation, 1970, 41: 899-91 2.

[0054] While the present invention has been described above in relation to its preferred embodiment, various modifications may be made thereto that still fall within the invention's scope, as would be recognized by those of ordinary skill in the art. Such modifications to the invention will be recognizable upon review of the teachings herein.

[0055] For example, one could divide the volume between the torso surface and the heart surface into several compartments corresponding to the lungs, fat, bones, and so on, and apply MFS ECGI within each of these compartments. After doing so, the results for all of the compartments can be combined to obtain the reconstruction of epicardial cardiac surface potentials.

[0056] The inventors also believe that meshless techniques other than the MFS technique described herein can be used to practice meshless noninvasive ECGI in accordance with the present invention; these alternative meshless techniques include but are not limited to other implementations of MFS (such as MFS implementations using dipoles or multi-poles of higher order), the Radial Basis Function (RBF), the Boundary Knot (BKM) method, the Meshless Local Petrov-Galerkin (MLPG) method, the Trefftz method, the Element Free Galerkin (ELG) method, the Partition of Unity method (PUM, including PUFEM, GFEM and XFEM), and the Meshless Finite Element method (MFEM).

[0057] Further still, the inventors note that practitioners may utilize different configurations of source nodes, different inverse matrix calculation methods (including all orders of Tikhonov regularization), different segmentation techniques, different geometry determining devices or make other changes, none of which belonging to the present invention, as would be understood by a person having ordinary skill in the art following the teachings set forth herein. As such, the specific examples described in the specification correspond to preferred embodiments and are not meant to limit the invention beyond that which is claimed.

[0058] Additional information pertaining to ECGI, its principles of operation, and meshless algorithms can be found in the following publications:

- Burnes et al., "A Noninvasive Imaging Modality for Cardiac Arrythmias", Circulation, pp. 2152-2158, October 24, 2000;
- Eisenberg, Anne, "Beyond the EKG, to a Hypersensitive Heart Monitor", The New York Times, April 22, 2004;
- Fairweather and Johnston, "The method of fundamental solutions for problems in potential theory", Treatment of Integral Equations by Numerical Methods, eds. Baker and Miller, Academic Press, London, pp. 349-359, 1982;
- Fries and Matthies, "Classification and Overview of Meshfree Methods", Institute of Scientific Computing, Technical University Braunschweig, Brunswick, Germany, Informatikbericht Nr.: 2003-3, July 2004 (revised);
- Ghanem et al., "Heart-Surface Reconstruction and ECG Electrodes Localization Using Fluoroscopy, Epipolar Geometry and Stereovision: Application to Noninvasive Imaging of Cardiac Electrical Activity", IEEE Transactions on Medical Imaging, Vol. 22, No. 10, pp. 1307-1318, October 2003;
- Golberg et al., "The method of fundamental solutions for diffusion equations", Boundary Element Technology XIII, eds. C.S. Chen,
- Wang and Rudy, "Application of the Method of Fundamental Solutions to Potential-based Inverse Electrocardiography", (expected to be published in the Annals of Biomedical Engineering in or around August 2006);

Appendix A:

[0059] The method of fundamental solution (MFS) has been used in various mathematical and engineering applications to compute solutions of partial differential equations (PDE). See Y. C. Hon, T. Wei, A fundamental solution method for inverse heat conduction problem, Engineering Analysis with Boundary Elements, Vol. 28, Issue 5, pp. 489-495, 2004; Fairweather G, R. L. Johnston, The method of fundamental solutions for problems in fluid flow, Appl. Math. Modeling, 8, 265-270, 1984; and Golberg MA, Chen CS. The method of fundamental solutions for potential, Helmholtz and diffusion problems. In Boundary Integral Methods, Golberg MA ed. Computational Mechanics Publications, 103-176, 1998.

[0060] MFS approximates the solution of a PDE by a linear combination of fundamental solutions of the governing

partial differential operator. See, Fairweather G, Karageorghis A. The method of fundamental solutions for elliptic boundary value problems. Adv Comput Math 9(1-2): 69-95, 1998. For ECGI, the governing partial differential operator is the Laplacian operator ∇^2. The formulation of MFS for a ∇^2 boundary value problem is described below.

[0061] MFS has evolved from traditional boundary integral methods. The following example is used to describe the theoretical formulation of MFS for a Laplacian operator.

$$\nabla^2 u(x) = 0, x \in \Omega \tag{a1}$$

$$u(x) = b(x),\ x \in \Gamma,\quad \Gamma = \partial\Omega \tag{a2}$$

where ∇^2 is the Laplace differential operator with a known fundamental solution $f(r)$ in 3D space, and where $b(x)$ is the Essential boundary condition. According to the definition of fundamental solution, the fundamental solution of the Laplace operator can be obtained by solving the following equations:

$$\nabla^2 f(r) = \delta(r) \tag{a3}$$

where $\delta(r)$ is the delta function, where $r = \|x - y\|$ is the 3D Euclid distance between point x and point y, and where $x, y \in \Omega$;

[0062] According to Kythe PK, Fundamental Solutions for Differential Operators and Applications, Birkhauser: Boston, Basel, Berlin. 1996, the entire disclosure of which is incorporated herein by reference:

$$f(r) = \begin{cases} -\dfrac{1}{2\pi}\ln r & ,2D \\ \dfrac{1}{4\pi r} & ,3D \end{cases} \tag{a4}$$

[0063] The traditional boundary integral approach is to represent solution u(x) in term of the double layer potential:

$$u(x) = \int_\Gamma \frac{\partial f(\|x-y\|)}{\partial n} e(y)dy,\quad x \in \Omega,\quad y \in \Gamma \tag{a5}$$

where, n is the outward pointing normal at point y, and where $e(y)$ is the unknown density function. See Patridge, P.W.,Brebbia, C.A.&Wrobel,L.C., The Dual Reciprocity Boundary Element Method, Computational Mechanics Publications, Southampton and Elsevier, London, 1992; and Golberg, M.A., Chen, C.S., Discrete Projection Methods for Integral Equations, Computational Mechanics Publications, Southampton, 1996. In recent years, the single layer potential representation of $u(x)$ for (a1)-(a2) has appeared in a substantial amount of work:

$$u(x) = \int_\Gamma f(\|x-y\|)e(y)dy,\quad x \in \Omega,\quad y \in \Gamma \tag{a6}$$

See Golberg, M.A., Chen, C.S., Discrete Projection Methods for Integral Equations, Computational Mechanics Publications, Southampton, 1996; Chen, Y., Atkinson, K.E., Solving a Single Layer Integral Equation on Surface in R3, the University of Iowa, Department of Mathematics, Technical Report, No 51, 1994.

[0064] The source density distribution $e(y)$ can be determined by solving the following equation under the assumption of a double layer:

$$\int_\Gamma \frac{\partial f(\|x-y\|)}{\partial n} e(y)dy = b(x),\quad x \in \Gamma,\quad y \in \Gamma \tag{a7}$$

or under the assumption of a single layer:

$$\int_\Gamma f(\|x-y\|)e(y)dy = b(x),\quad x \in \Gamma,\quad y \in \Gamma \tag{a8}$$

[0065] However the singular integrals are involved in both cases, which become the most difficult part in solving the problem. To alleviate the difficulties of singular integrals, the following formulation (similar to the single layer potential in (a6)) was considered in Karageorghis, A., Fairweather, G., The method of fundamental solutions for the numerical solution of the biharmonic equation, Journal of Computational Physics, 69, 435-459, 1987, i.e.,

$$u(x) = \int_{\hat{\Gamma}} f(\|x-y\|)e(y)dy, \quad x \in \Omega, \quad y \in \hat{\Gamma} \tag{a9}$$

where boundary $\hat{\Gamma}$ is the surface of the domain $\hat{\Omega}$ containing Ω as shown below.

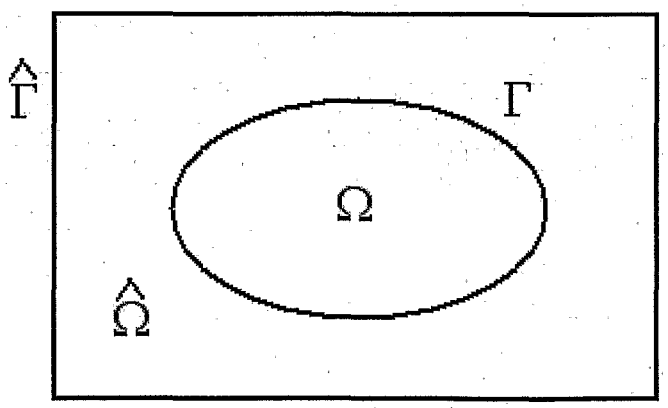

[0066] Because $f(\|x-y\|)$ is the fundamental solution of the Laplace operator as shown in equation (a3), (a9) satisfies the differential Equation (a1) automatically. Therefore we need only to force the boundary condition (a2), which means:

$$\int_{\hat{\Gamma}} f(\|x-y\|)e(y)dy = b(x), \quad x \in \Gamma, \quad y \in \hat{\Gamma} \tag{a10}$$

where source density distribution $e(y)$, $y \in \hat{\Gamma}$, is to be determined. Once the source density is determined, the solution of (a1)-(a2) is solved. The analytic integral representation of (a10) means that there are infinite number of source density points on $\hat{\Gamma}$. Therefore, in order to apply numerical solution method, it is necessary to discretize $e(y)$.

[0067] Assume $\Psi_j(y)$, $j = 1,2,\cdots \infty$ is a complete set of functions on $\hat{\Gamma}$, $e(y)$ can be approximated by:

$$e(y) = \sum_{j=1}^{n} c_j \psi_j(y), \quad y \in \hat{\Gamma} \tag{a11}$$

Substituting (a11) into (a10) and collocating at n points on $x_k \in \Gamma$, $k = 1,2,\cdots n$; we have

$$\sum_{j=1}^{n} c_j \int_{\hat{\Gamma}} f(\|x_k - y\|)\psi_j(y)dy = b(x_k), \quad 1 \le k \le n, \quad y \in \hat{\Gamma} \tag{a12}$$

Since the fictitious boundary $\hat{\Gamma}$ located outside the physical domain, the integrand $f(\|x_k-y\|)$ is nonsingular and standard quadrature rules can be used giving

$$\int_{\hat{\Gamma}} f(\|x_k - y\|)\psi_j(y)dy \approx \sum_{i=1}^{M} w_i f(\|x_k - y_i\|)\psi_j(y), \quad y_i \in \hat{\Gamma}, \quad i = 1,2,...,M \tag{a13}$$

From (a12) and (a13), we can obtain:

$$\sum_{j=1}^{n} c_j \sum_{i=1}^{M} w_i f(\|x_k - y_i\|)\psi_j(y_i) = \sum_{i=1}^{M} w_i \left[\sum_{j=1}^{n} c_j \psi_j(y_i)\right] f(\|x_k - y_i\|) = b(x_k), \quad 1 \le k \le n. \tag{a14}$$

Then:

$$\sum_{i=1}^{M} a_i f(\|x_k - y_i\|) = b(x_k), \quad 1 \le k \le n. \tag{a15}$$

where source density distribution $e(y)$, $y \in \hat{\Gamma}$, is to be determined. Once the source density is determined, the solution of (a1)-(a2) is solved. The analytic integral representation of (a10) means that there are infinite number of source density points on $\hat{\Gamma}$. Therefore, in order to apply numerical solution method, it is necessary to discretize $e(y)$.

[0068] Assume $\psi_j(y)$, $j = 1,2,\cdots \infty$ is a complete set of functions on $\hat{\Gamma}$, $e(y)$ can be approximated by:

$$e(y) = \sum_{j=1}^{n} c_j \psi_j(y), \quad y \in \hat{\Gamma} \tag{a11}$$

Substituting (a11) into (a10) and collocating at n points on $x_k \in \Gamma, k = 1,2,\cdots n$; we have

$$\sum_{j=1}^{n} c_j \int_{\hat{\Gamma}} f(\|x_k - y\|)\psi_j(y)dy = b(x_k), \quad 1 \le k \le n, \quad y \in \hat{\Gamma} \tag{a12}$$

Since the fictitious boundary $\hat{\Gamma}$ located outside the physical domain, the integrand $f(\|x_k\text{-}y\|)$ is nonsingular and standard quadrature rules can be used giving

$$\int_{\hat{\Gamma}} f(\|x_k - y\|)\psi_j(y)dy \approx \sum_{i=1}^{M} w_i f(\|x_k - y_i\|)\psi_j(y), \quad y_i \in \hat{\Gamma}, \quad i = 1,2,...,M \tag{a13}$$

From (a12) and (a13), we can obtain:

$$\sum_{j=1}^{n} c_j \sum_{i=1}^{M} w_i f(\|x_k - y_i\|)\psi_j(y_i) = \sum_{i=1}^{M} w_i \left[\sum_{j=1}^{n} c_j \psi_j(y_i)\right] f(\|x_k - y_i\|) = b(x_k), \quad 1 \le k \le n. \tag{a14}$$

Then:

$$\sum_{i=1}^{M} a_i f(\|x_k - y_i\|) = b(x_k), \quad 1 \le k \le n. \tag{a15}$$

where:

$$a_i = w_i \sum_{j=1}^{n} c_j \psi_j(y_i) \qquad \text{(a16)}$$

We can find (a15) is equivalent to approximate the solution to (a1) by

$$u_a(x) = \sum_{j=1}^{M} a_j f(\|x - y_j\|), \quad x \in \Gamma, \quad y_j \in \hat{\Gamma} \qquad \text{(a17)}$$

For completeness, a constant coefficient is added into (17):

$$u_a(x) = a_0 + \sum_{j=1}^{M} a_j f(\|x - y_j\|), \quad x \in \Gamma, \quad y_j \in \hat{\Gamma} \qquad \text{(a18)}$$

[0069] The above mathematical formulation (a18) is referred to as Method of Fundamental Solution (MFS). See Golberg MA, Chen CS. The method of fundamental solutions for potential, Helmholtz and diffusion problems. In Boundary Integral Methods, Golberg MA ed. Computational Mechanics Publications, 103-176, 1998. As we can see in (a 18), the approximate solution u_α can be represented by a linear combination of fundamental solutions of the governing equation with the singularities y_j, j = 1,2, ⋯M. placed outside the domain of the problem.

[0070] It is important to note that the MFS is applicable to different types of boundary conditions. For Natural boundary condition, if the point x lies on the boundary of solution domain, then the gradient along the outward normal to the boundary at x is given by:

$$\frac{\partial}{\partial n} u_a(x) = \sum_{j=1}^{M} a_j \frac{\partial}{\partial n} f(\|x - y_j\|), \quad x \in \Gamma, \quad y_j \in \hat{\Gamma}. \qquad \text{(a19)}$$

Therefore the Natural boundary condition:

$$\frac{\partial}{\partial n} u(x) = i(x), \quad x \in \Gamma, \quad \Gamma = \partial\Omega \qquad \text{(a20)}$$

can be discretized and expressed as:

$$\sum_{i=1}^{M} a_i \frac{\partial}{\partial n} f(\|x_k - y_j\|) = i(x_k), \quad x_k \in \Gamma, \quad k = 1,2,...,n, \quad y_j \in \hat{\Gamma}, \quad j = 1,2,...,M; \qquad \text{(a21)}$$

Appendix B:

[0071] For the tank-torso protocols, statistical measurements in terms of relative error (RE) and correlation coefficients (CC) were computed with respect to the measured data to quantitatively evaluate the accuracy of ECGI. RE gives an estimate of the amplitude difference and CC gives an estimate of the similarity of potential patterns or electrogram morphologies between the measured and computed data:

$$RE = \sqrt{\frac{\sum_{i=1}^{n} (V_i^C - V_i^M)^2}{\sum_{i=1}^{n} (V_i^M)^2}}$$

$$CC = \frac{\sum_{i=1}^{n}(V_i^M - \overline{V}^M)(V_i^C - \overline{V}^C)}{\sqrt{\sum_{i=1}^{n}(V_i^M - \overline{V}^M)^2}\sqrt{\sum_{i=1}^{n}(V_i^C - \overline{V}^C)^2}}$$

where n is the number of nodes (points at which epicardial potentials are computed). For electrograms, n is the number of time frames. V_i^C is the computed potential for node *i*, V_i^M is the measured potential for node *i*, $\overline{V}^M$ is the average measured potential, and $\overline{V}^C$ is the average computed potential.

[0072] In addition to CC and RE, pacing site localization errors (distance between computed and measured locations) are also provided for both torso-tank and human reconstructions. The computed pacing site location was estimated by the center of an ellipse that best fits the quasi-elliptical negative potential region that develops around the pacing site. The earliest time frame after pacing, for which such pattern was present, was used for this purpose. Pacing sites could also be determined from isochrone maps as the sites of earliest activation.

[0073] Qualitative evaluations of ECGI reconstructions are conducted by visual comparison to measured data (torso-tank experiments) and to well established potentials, electrograms and isochrone patterns associated with pacing (human subjects).

[0074] In addition to CC RE, clinical application of ECGI will benefit from computational efficiency that reconstructs epicardial potentials in close to real time (near real time). Although regularization procedures (e.g. Tikhonov regularization with the regularization parameter selected by CRESO, and so on) can be done close to real-time, forming the coefficient matrix usually still takes more than 1 minute in BEM ECGI. Ideally if the coefficient matrix can also be formed within less time (e.g. less than one second), ECGI would have much better chance to be used in the interactive applications during clinical interventions. In order to evaluate the speed of forming the coefficient matrix for BEM ECGI and MFS ECGI, Computation Time (CT) and Computation Time Ratio (CTR) between MFS ECGI and BEM ECGI are defined as:
CT = Computation time of forming coefficient matrix (in seconds)

$$\mathrm{CTR} = \frac{\mathrm{CT\ of\ BEM\ ECGI}}{\mathrm{CT\ of\ MFS\ ECGI}}$$

[0075] CT and CRT were computed on a laptop with Pentium Mobile 1.7GHz and 1G RAM. Qualitative evaluations of automatic between MFS ECGI and BEM ECGI were also done by comparing the working procedure of MFS ECGI and BEM ECGI in specific cases.

Claims

1. A noninvasive system (100) for determining electrical activity for a heart of a living being, the system comprising:

a processor (114);
an electrode array system (102) in communication with the processor (114) for noninvasively measuring electrical potentials at a plurality of locations on a torso of a living being via a plurality of electrodes (104) applied to the torso and providing a set of body surface electrical potentials;
a geometry determining device (116) in communication with the processor, the geometry determining device being configured to generate geometry data that is indicative of a geometrical relationship between a plurality of locations corresponding to the nodes where the body surface electrical potentials were measured and nodes on an epicardial cardiac envelope of the heart;
characterized in that the processor (114) is configured to:

receive the set of body surface electrical potentials and the geometry data;
determine a plurality of epicardial nodes that define locations on the epicardial cardiac envelope;
determine a plurality of external source nodes that define a plurality of locations along a surface that is outside the torso of the living being;
determine a plurality of internal source nodes that define a plurality of locations along a surface inside the epicardial cardiac surface; and
use a method of fundamental solution (MFS) to reconstruct epicardial cardiac surface potentials for the

plurality of epicardial cardiac nodes from the set of body surface electrical potentials based on the geometry data by:

(1) determining a matrix of coefficients A (408) that relates each electrode location to each source node location, (2) performing an inverse computation on A (410) and the noninvasively measured body surface electrical potentials to compute a plurality of internal and external source node coefficients, (3) determining a matrix of coefficients B (414) that relates each epicardial node location to each internal and external source node location, and (4) performing a forward computation (416) using B and the source node coefficients to compute the reconstructed epicardial cardiac surface electrical potentials.

2. The system of claim 1 wherein the processor is further configured to statically determine the internal and external source nodes by (1) defining each external source node such that it is located a predetermined distance outward from a corresponding electrode location on a ray extending from a calculated center of the epicardial cardiac envelope through the corresponding electrode location, and (2) defining each internal source node such that it is located a predetermined distance inward from a corresponding epicardial node location on a ray extending from the calculated center of the epicardial cardiac envelope through the corresponding epicardial node location.

3. The system of claim 1 or 2 wherein the processor is further configured to generate an epicardial cardiac surface potential map from the set of computed epicardial cardiac surface electrical potentials.

4. The system of any of claims 1 or 2 wherein the processor is further configured to compute a plurality of sets of the epicardial cardiac surface electrical potentials over a time duration from a plurality of successively noninvasively measured body surface electrical potentials.

5. The system of claim 4 wherein the processor is further configured to generate at least one selected from the group consisting of a plurality of electrograms and an isochrone from the sets of computed epicardial cardiac surface electrical potentials.

6. The system of claim 4 wherein the processor is further configured to generate, from the sets of computed epicardial cardiac surface electrical potentials, at least one selected from the group consisting of a recovery map, an integral map, and an activation-recovery interval map.

Patentansprüche

1. Nichtinvasives System (100) zum Bestimmen einer elektrischen Aktivität eines Herzes eines Lebewesens, wobei das System Folgendes umfasst:

einen Prozessor (114);
ein Elektrodenarraysystem (102) in Kommunikation mit dem Prozessor (114) zum nichtinvasiven Messen elektrischer Potentiale an mehreren Positionen an einem Rumpf eines Lebewesens über mehrere Elektroden (104), die an den Rumpf angelegt sind, und Bereitstellen eines Satzes elektrischer Potentiale an der Körperoberfläche;
eine Geometriebestimmungsvorrichtung (116) in Kommunikation mit dem Prozessor, wobei die Geometriebestimmungsvorrichtung konfiguriert ist, um Geometriedaten zu erzeugen, die eine geometrische Beziehung zwischen mehreren Positionen anzeigen, die den Knoten, an denen die elektrischen Potentiale an der Körperoberfläche gemessen wurden, und Knoten an einer epikardialen Herzhülle des Herzes entsprechen;

dadurch gekennzeichnet, dass der Prozessor (114) für Folgendes konfiguriert ist: Empfangen des Satzes elektrischer Potentiale an der Körperoberfläche und der Geometriedaten;

Bestimmen mehrerer epikardialer Knoten, die Positionen auf der epikardialen Herzhülle definieren;
Bestimmen mehrerer externer Quellenknoten, die mehrere Positionen entlang einer Oberfläche definieren, die sich außerhalb des Rumpfes des Lebewesens befindet;
Bestimmen mehrerer interner Quellenknoten, die mehrere Positionen entlang einer Oberfläche innerhalb der epikardialen Herzoberfläche definieren; und
Verwenden eines Verfahrens der Fundamentallösung (*method of fundamental solution* - MFS), um die epikardialen Herzoberflächenpotentiale für die mehreren epikardialen Herzknoten aus dem Satz elektrischer Potentiale an der Körperoberfläche basierend auf den Geometriedaten durch Folgendes zu rekonstruieren:

(1)Bestimmen einer Koeffizientenmatrix A (408), die jede Elektrodenposition mit jeder Quellenknotenposition in Beziehung setzt, (2) Durchführen einer inversen Berechnung an A (410) und den nichtinvasiv gemessenen elektrischen Potentialen an der Körperoberfläche, um mehrere interne und externe Quellenknotenkoeffizienten zu berechnen, (3) Bestimmen einer Koeffizientenmatrix B (414), die jede epikardiale Knotenposition mit jeder internen und externen Quellenknotenposition in Beziehung setzt, und (4) Durchführen einer Vorwärtsberechnung (416) unter Verwendung von B und der Quellenknotenkoeffizienten, um die rekonstruierten elektrischen Potentiale an der epikardialen Herzoberfläche zu berechnen.

2. System nach Anspruch 1, wobei der Prozessor ferner konfiguriert ist, um den internen und den externen Quellenknoten statisch durch Folgendes zu bestimmen: (1) Definieren jedes externen Quellenknotens derart, dass er mit einem vorbestimmten Abstand nach außen von einer entsprechenden Elektrodenposition auf einem Strahl positioniert ist, der sich von einem berechneten Zentrum der epikardialen Herzhülle durch die entsprechende Elektrodenposition erstreckt, und (2) Definieren jedes internen Quellenknotens derart, dass er mit einem vorgegebenen Abstand nach innen von einer entsprechenden epikardialen Knotenposition auf einem Strahl positioniert ist, der sich von dem berechneten Zentrum der epikardialen Herzhülle durch die entsprechende epikardiale Knotenposition erstreckt.

3. System nach Anspruch 1 oder 2, wobei der Prozessor ferner konfiguriert ist, um eine epikardiale Herzoberflächenpotentialkarte aus dem Satz berechneter elektrischer Potentiale an der epikardialen Herzoberfläche zu erzeugen.

4. System nach einem der Ansprüche 1 und 2, wobei der Prozessor ferner konfiguriert ist, um mehrere Sätze elektrischer Potentiale an der epikardialen Herzoberfläche über einen Zeitraum aus mehreren aufeinanderfolgend nichtinvasiv gemessenen elektrischen Potentialen an der Körperoberfläche zu berechnen.

5. System nach Anspruch 4, wobei der Prozessor ferner konfiguriert ist, um mindestens eines zu erzeugen, das aus der Gruppe ausgewählt ist, die aus mehreren Elektrogrammen und einem Isochron der Sätze berechneter elektrischer Potentiale an der epikardialen Herzoberfläche besteht.

6. System nach Anspruch 4, wobei der Prozessor ferner konfiguriert ist, um aus den Sätzen berechneter elektrischer Potentiale an der epikardialen Herzoberfläche, mindestens eines zu erzeugen, das aus der Gruppe ausgewählt ist, die aus einer Wiederherstellungskarte, einer integralen Karte und einer Aktivierungs-Wiederherstellungs-Intervallkarte besteht.

Revendications

1. Système non invasif (100) pour déterminer l'activité électrique d'un cœur d'un être vivant, le système comprenant :

un processeur (114) ;
un système de réseau d'électrodes (102) en communication avec le processeur (114) pour mesurer de manière non invasive des potentiels électriques à une pluralité d'emplacements sur le torse d'un être vivant par l'intermédiaire d'une pluralité d'électrodes (104) appliquées sur le torse et fournissant un ensemble de potentiels électriques à la surface du corps ;
un dispositif de détermination de géométrie (116) en communication avec le processeur, le dispositif de détermination de géométrie étant configuré pour générer des données de géométrie indiquant une relation géométrique entre une pluralité d'emplacements correspondant aux nœuds où les potentiels électriques de surface du corps ont été mesurés et les nœuds sur une enveloppe cardiaque épicardique du cœur ;

caractérisé en ce que le processeur (114) est configuré pour :

recevoir l'ensemble de potentiels électriques de surface du corps et les données de géométrie ;
déterminer une pluralité de nœuds épicardiques définissant des emplacements sur l'enveloppe cardiaque épicardique ;
déterminer une pluralité de nœuds sources externes qui définissent une pluralité d'emplacements le long d'une surface qui est à l'extérieur du torse de l'être vivant ;

déterminer une pluralité de nœuds sources internes qui définissent une pluralité d'emplacements le long d'une

surface à l'intérieur de la surface cardiaque épicardique ; et
utiliser une méthode des solutions fondamentales (MFS) pour reconstruire les potentiels de surface cardiaques épicardiques pour la pluralité de nœuds cardiaques épicardiques à partir de l'ensemble des potentiels électriques de surface corporelle, sur la base des données géométriques, en :

(1) déterminant une matrice de coefficients A (408) qui relie chaque emplacement d'électrode à chaque emplacement de nœud source, (2) effectuant un calcul inverse sur A (410) et les potentiels électriques de surface corporelle mesurés de manière non invasive pour calculer une pluralité de nœuds source interne et externe des coefficients, (3) déterminant une matrice de coefficients B (414) reliant chaque emplacement de nœud épicardique à chaque emplacement de nœud source interne et externe, et (4) effectuant un calcul direct (416) en utilisant B et les coefficients de nœud source pour calculer les potentiels électriques de surface cardiaque épicardique reconstruits.

2. Système selon la revendication 1, dans lequel le processeur est en outre configuré pour déterminer statiquement les nœuds sources interne et externe (1) en définissant chaque nœud source externe de telle sorte qu'il est situé à une distance prédéterminée vers l'extérieur à partir d'un emplacement d'électrode correspondant sur un rayon s'étendant à partir d'un centre calculé de l'enveloppe cardiaque épicardique à travers l'emplacement d'électrode correspondant, et (2) définissant chaque nœud source interne de telle sorte qu'il se trouve à une distance prédéterminée vers l'intérieur d'un emplacement de nœud épicardique correspondant sur un rayon s'étendant à partir du centre calculé de l'enveloppe cardiaque épicardique à travers l'emplacement du nœud épicardique correspondant.

3. Système selon la revendication 1 ou 2, dans lequel le processeur est en outre configuré pour générer une carte de potentiel de surface cardiaque épicardique à partir de l'ensemble des potentiels électriques de surface cardiaque épicardique calculés.

4. Système selon l'une quelconque des revendications 1 ou 2, dans lequel le processeur est en outre configuré pour calculer une pluralité d'ensembles des potentiels électriques de surface cardiaque épicardiques sur une durée à partir d'une pluralité de potentiels électriques de surface corporelle successivement mesurés de manière non invasive.

5. Système selon la revendication 4, dans lequel le processeur est en outre configuré pour générer au moins un élément sélectionné dans le groupe constitué d'une pluralité d'électrogrammes et d'une isochrone à partir des ensembles de potentiels électriques de surface cardiaque épicardique calculés.

6. Système selon la revendication 4, dans lequel le processeur est en outre configuré pour générer, à partir des ensembles de potentiels électriques de surface cardiaque épicardique calculés, au moins un élément choisi dans le groupe constitué par une carte de récupération, une carte intégrale et une carte d'intervalle activation/récupération.

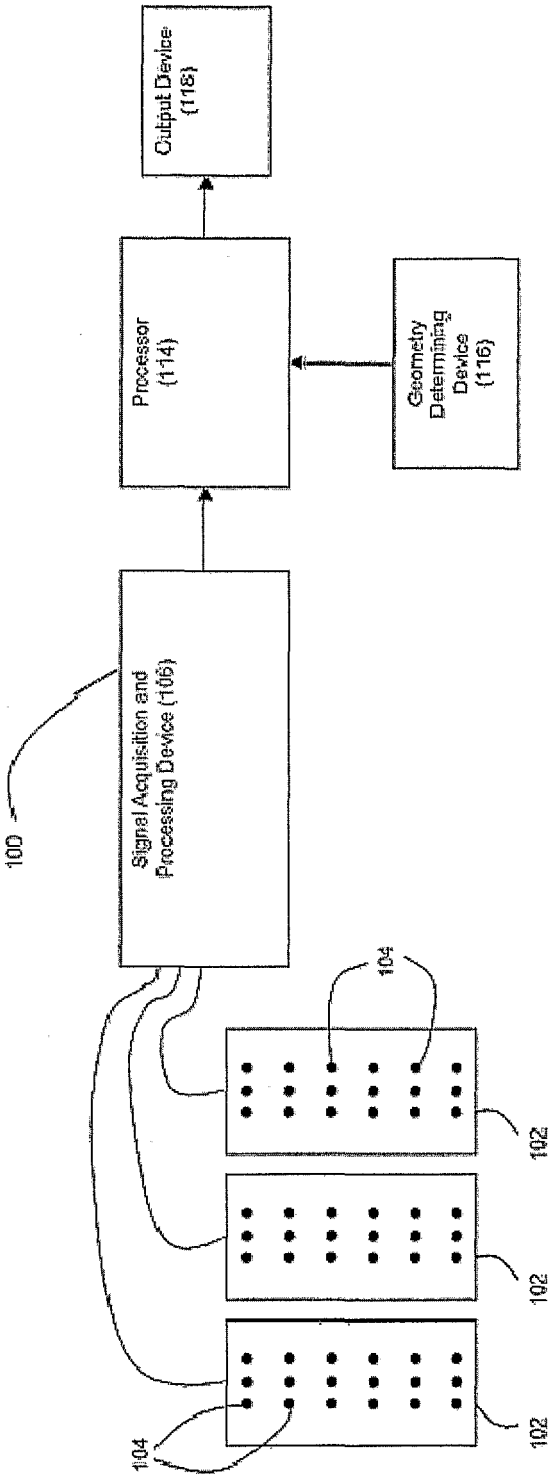

Figure 1

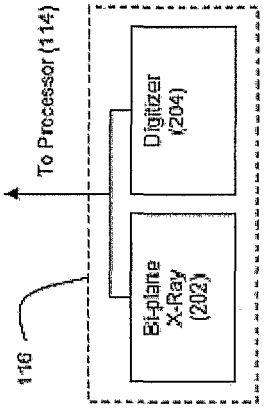

Figure 2(b)

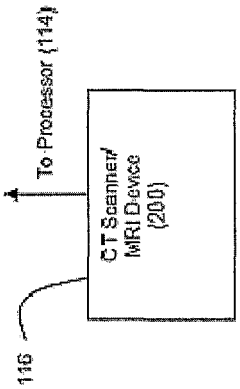

Figure 2(a)

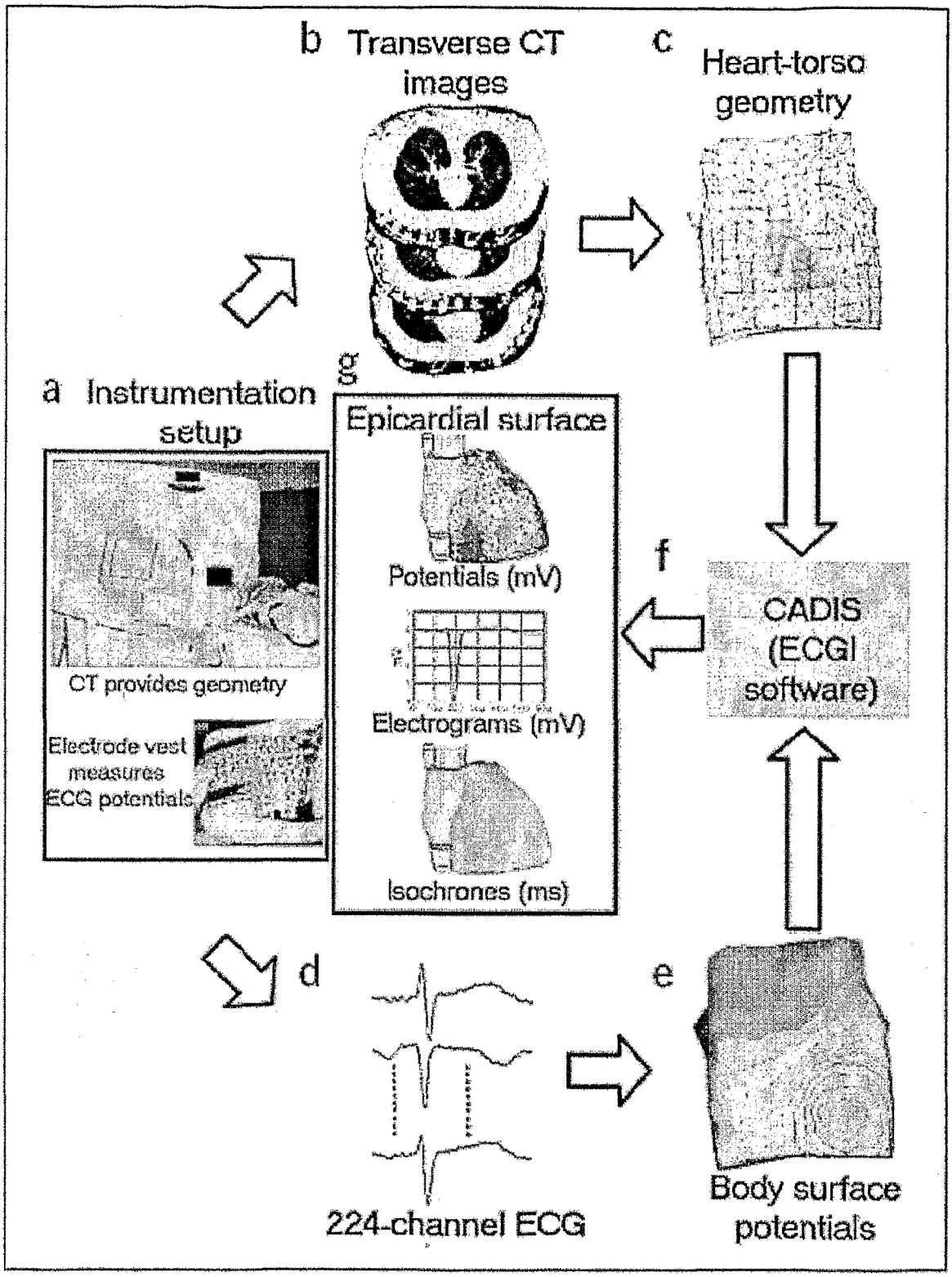
b Transverse CT images
c Heart-torso geometry
a Instrumentation setup
g
Epicardial surface
Potentials (mV)
Electrograms (mV)
Isochrones (ms)
CT provides geometry
Electrode vest measures ECG potentials
f
CADIS (ECGI software)
d
e
224-channel ECG
Body surface potentials

Figure 3

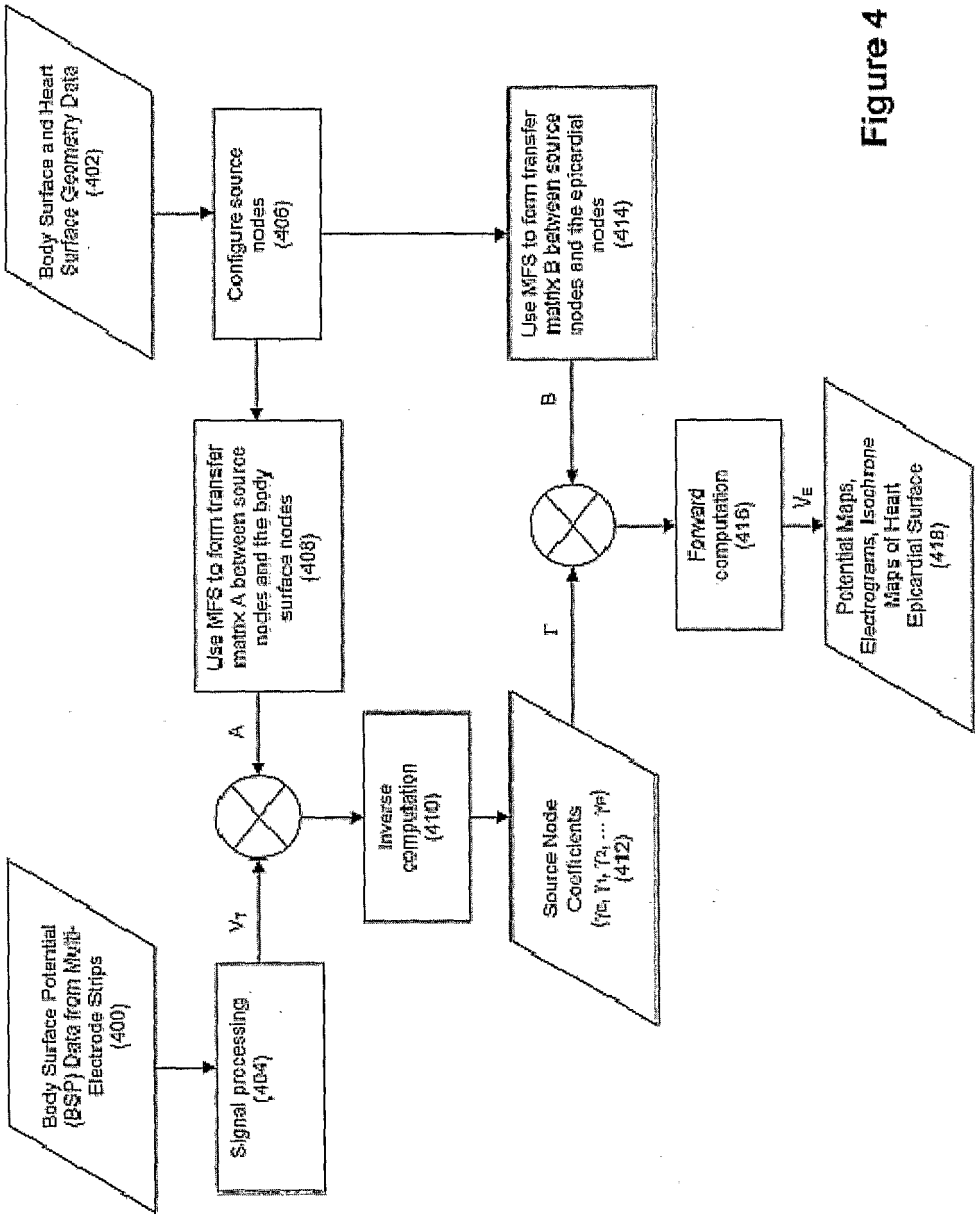
Body Surface and Heart Surface Geometry Data (402)
Configure source nodes (406)
Use MFS to form transfer matrix A between source nodes and the body surface nodes (408)
Use MFS to form transfer matrix B between source nodes and the epicardial nodes (414)
Body Surface Potential (BSP) Data from Multi-Electrode Strips (400)
Signal processing (404)
V_T
A
Inverse computation (410)
Source Node Coefficients ($\gamma_0, \gamma_1, \gamma_2 \ldots \gamma_P$) (412)
Γ
B
Forward computation (416)
V_E
Potential Maps, Electrograms, Isochrone Maps of Heart Epicardial Surface (418)

Figure 4

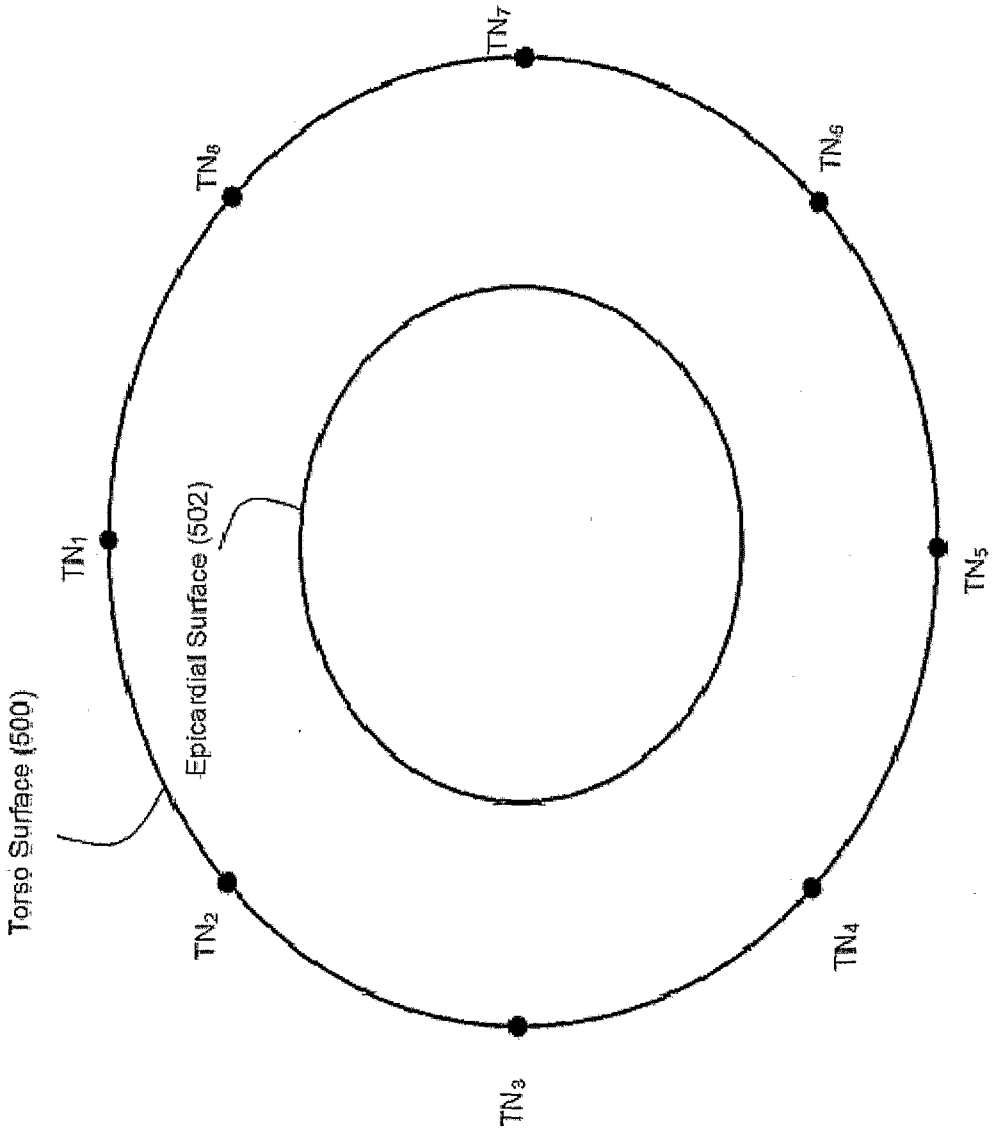
TN7
TN6
TN5
TN4
TN3
TN2
TN1
TN8
Epicardial Surface (502)
Torso Surface (500)

Figure 5(a)

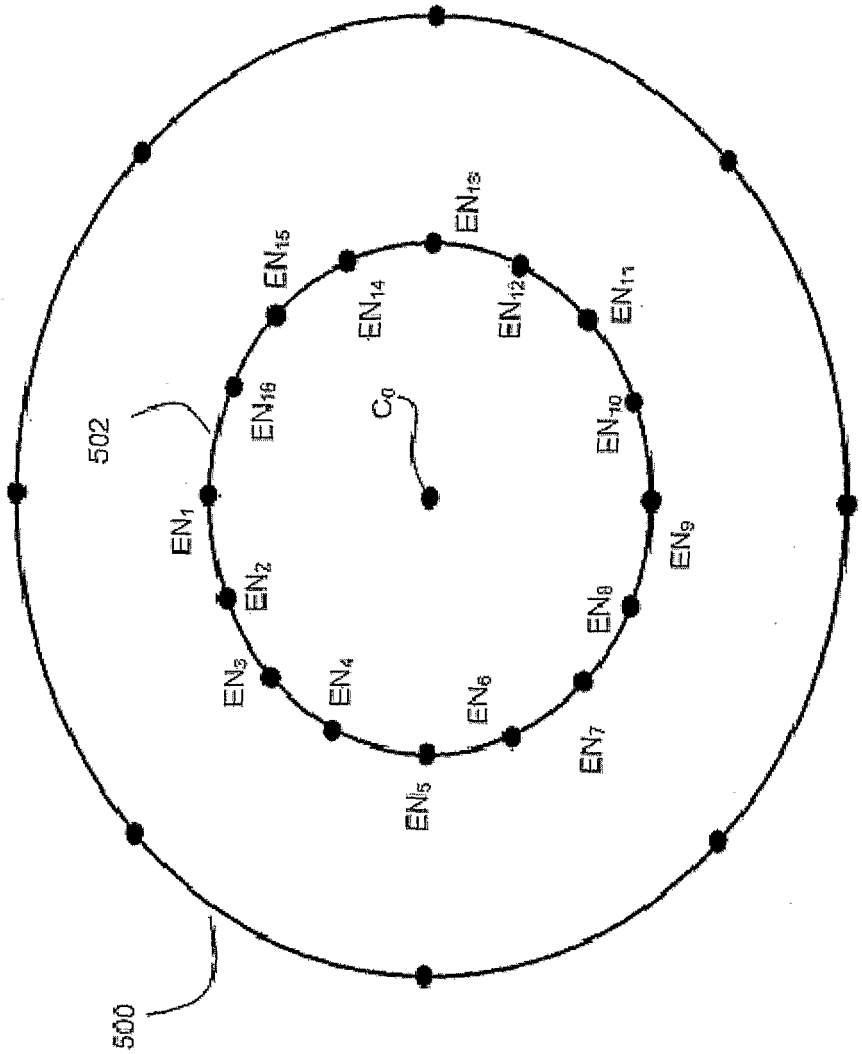
500
502
EN1
EN2
EN3
EN4
EN5
EN6
EN7
EN8
EN9
EN10
EN11
EN12
EN13
EN14
EN15
EN16
C0

Figure 5(b)

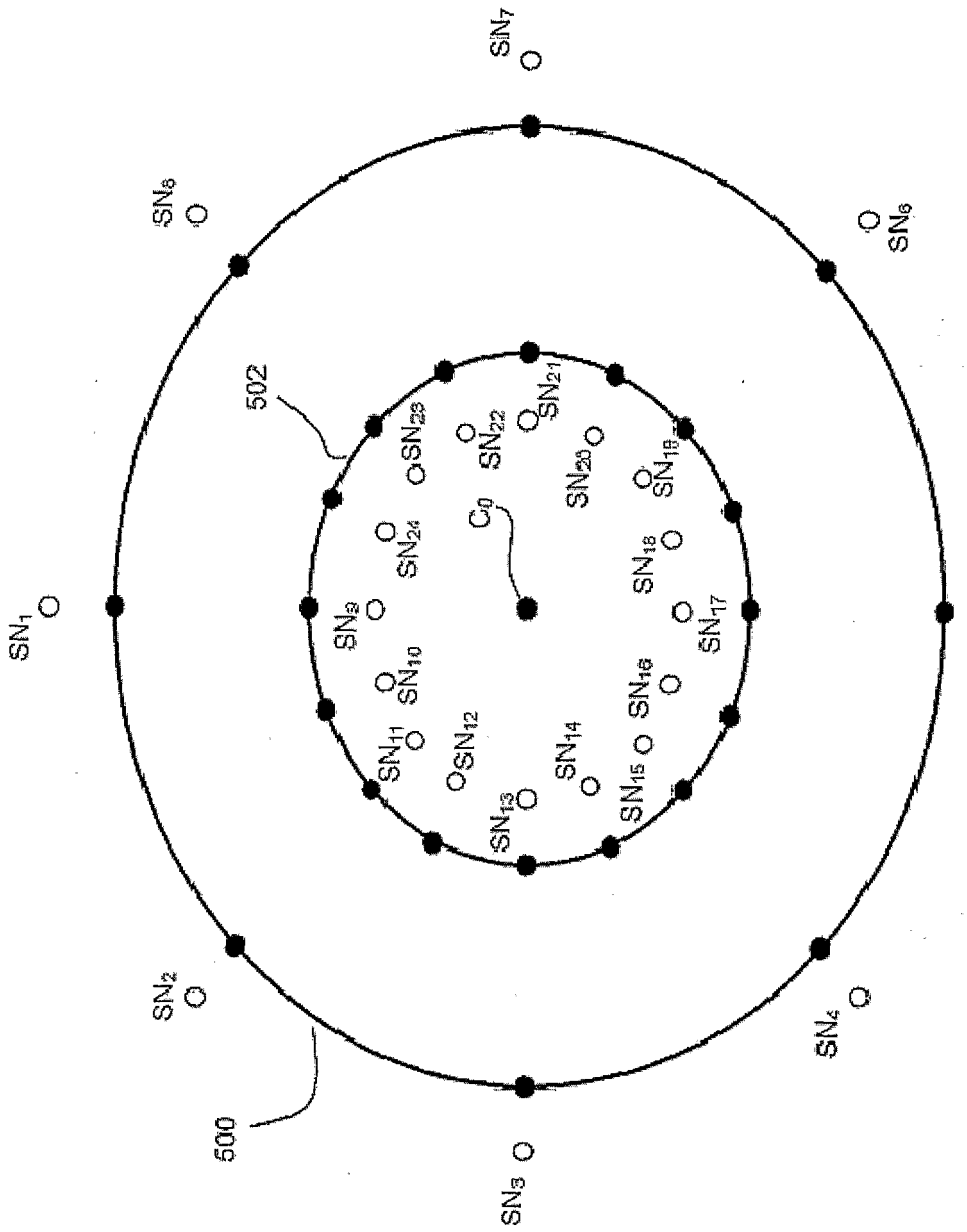
SN1
SN2
SN3
SN4
SN5
SN6
SN7
SN8
500
502
C0
SN9
SN10
SN11
SN12
SN13
SN14
SN15
SN16
SN17
SN18
SN19
SN20
SN21
SN22
SN23
SN24

Figure 5(c)

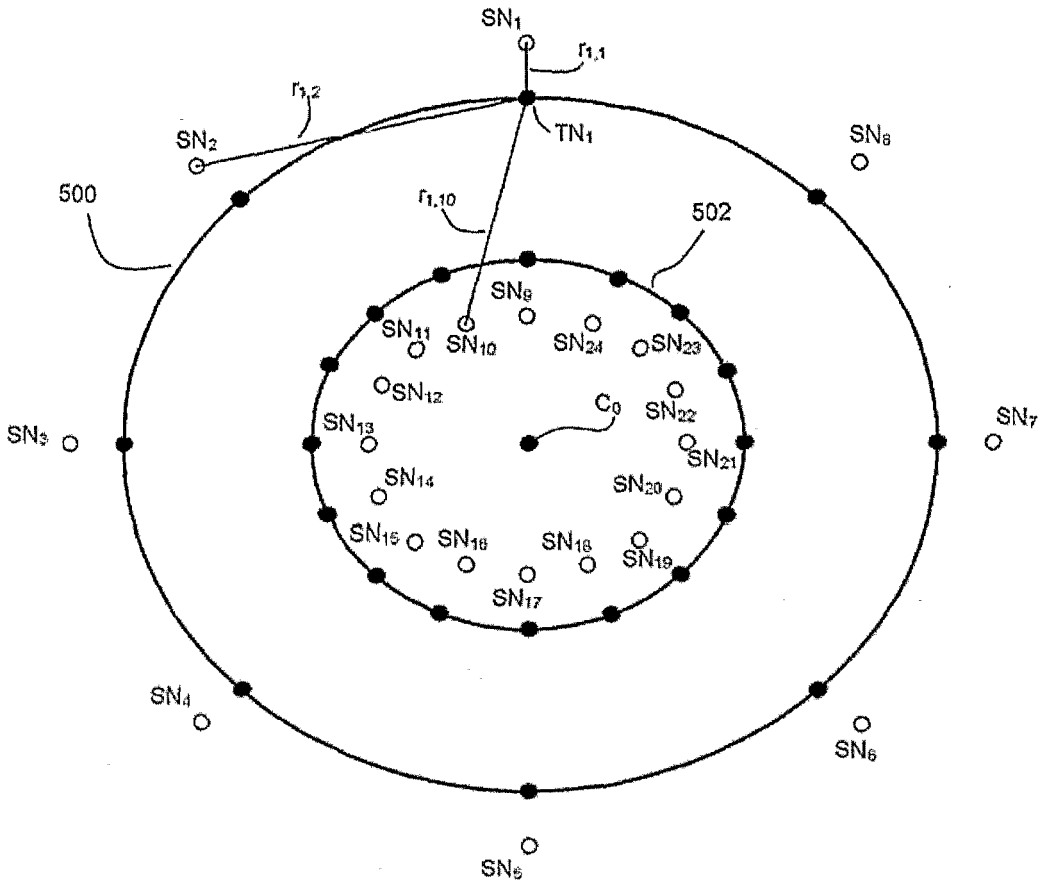

Figure 5(d)

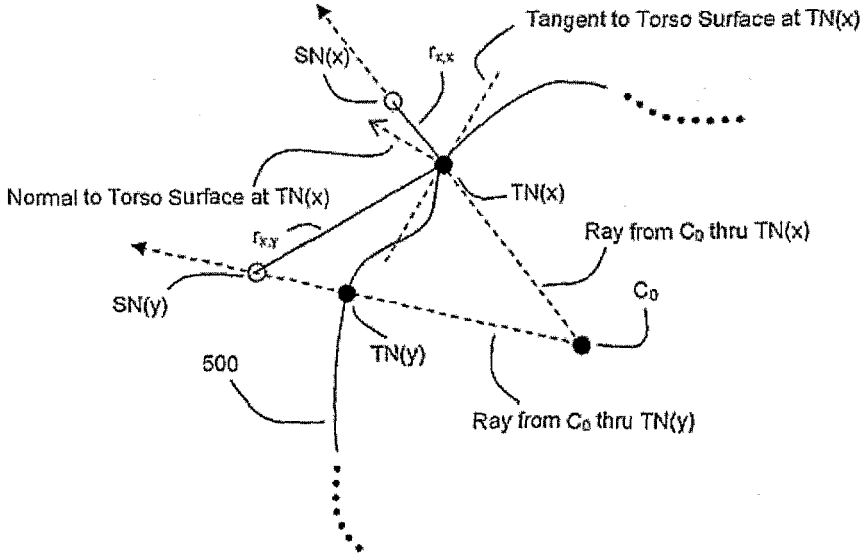

Figure 5(e)

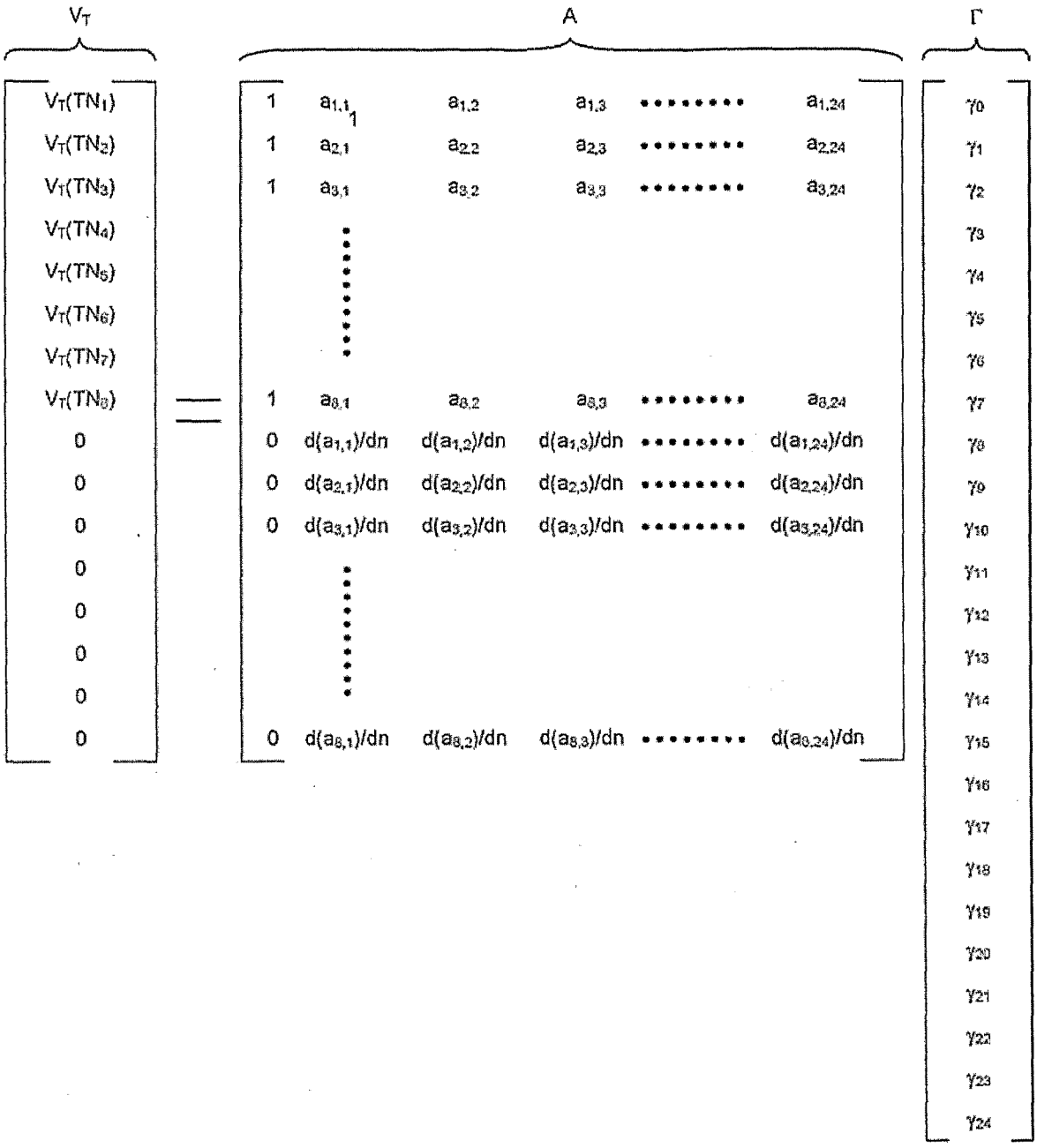
V_T
A
Γ
$V_T(TN_1)$
$V_T(TN_2)$
$V_T(TN_3)$
$V_T(TN_4)$
$V_T(TN_5)$
$V_T(TN_6)$
$V_T(TN_7)$
$V_T(TN_8)$
0
0
0
0
0
0
0
0
=
1 $a_{1,1}$ $a_{1,2}$ $a_{1,3}$ ••••••••• $a_{1,24}$
1 $a_{2,1}$ $a_{2,2}$ $a_{2,3}$ ••••••••• $a_{2,24}$
1 $a_{3,1}$ $a_{3,2}$ $a_{3,3}$ ••••••••• $a_{3,24}$
1 $a_{8,1}$ $a_{8,2}$ $a_{8,3}$ ••••••••• $a_{8,24}$
0 $d(a_{1,1})/dn$ $d(a_{1,2})/dn$ $d(a_{1,3})/dn$ ••••••••• $d(a_{1,24})/dn$
0 $d(a_{2,1})/dn$ $d(a_{2,2})/dn$ $d(a_{2,3})/dn$ ••••••••• $d(a_{2,24})/dn$
0 $d(a_{3,1})/dn$ $d(a_{3,2})/dn$ $d(a_{3,3})/dn$ ••••••••• $d(a_{3,24})/dn$
0 $d(a_{8,1})/dn$ $d(a_{8,2})/dn$ $d(a_{8,3})/dn$ ••••••••• $d(a_{8,24})/dn$
γ_0 γ_1 γ_2 γ_3 γ_4 γ_5 γ_6 γ_7 γ_8 γ_9 γ_{10} γ_{11} γ_{12} γ_{13} γ_{14} γ_{15} γ_{16} γ_{17} γ_{18} γ_{19} γ_{20} γ_{21} γ_{22} γ_{23} γ_{24}

Figure 6

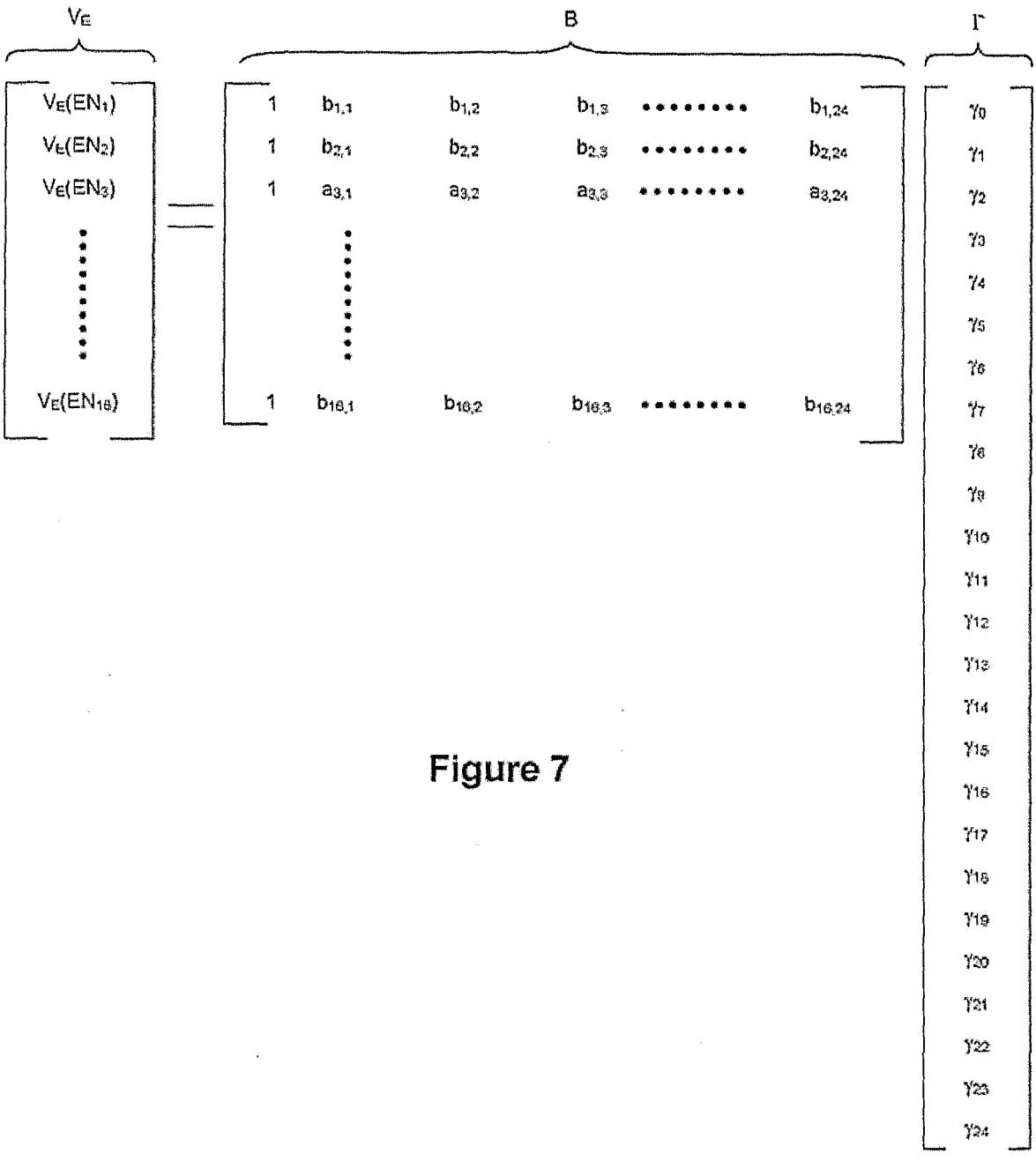
VE
B
Γ
VE(EN1)
VE(EN2)
VE(EN3)
VE(EN16)
1 b1,1 b1,2 b1,3 ..... b1,24
1 b2,1 b2,2 b2,3 ..... b2,24
1 a3,1 a3,2 a3,3 ..... a3,24
1 b16,1 b16,2 b16,3 ..... b16,24
γ0 γ1 γ2 γ3 γ4 γ5 γ6 γ7 γ8 γ9 γ10 γ11 γ12 γ13 γ14 γ15 γ16 γ17 γ18 γ19 γ20 γ21 γ22 γ23 γ24

Figure 7

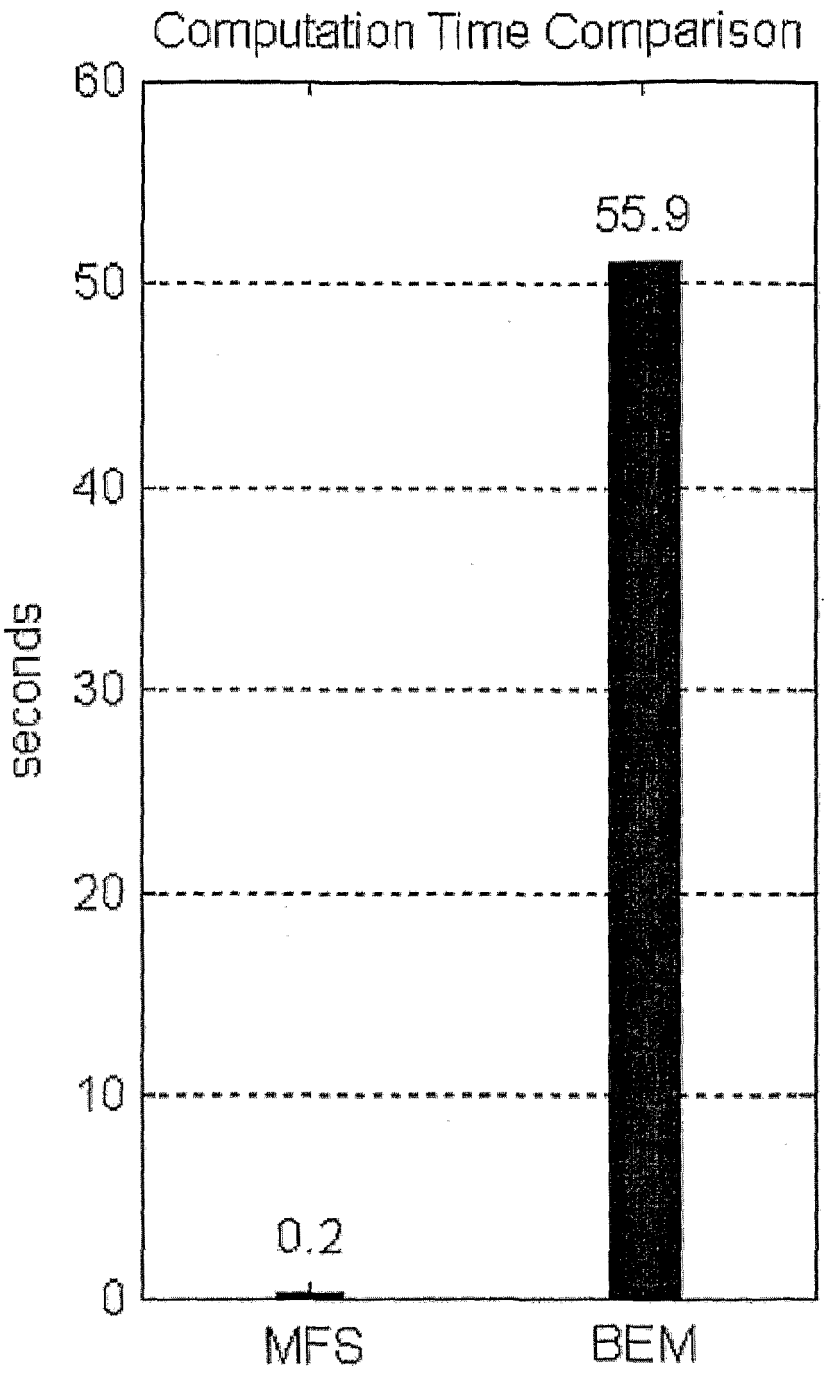
Computation Time Comparison
60
50
40
30
20
10
0
seconds
55.9
0.2
MFS
BEM

Figure 8

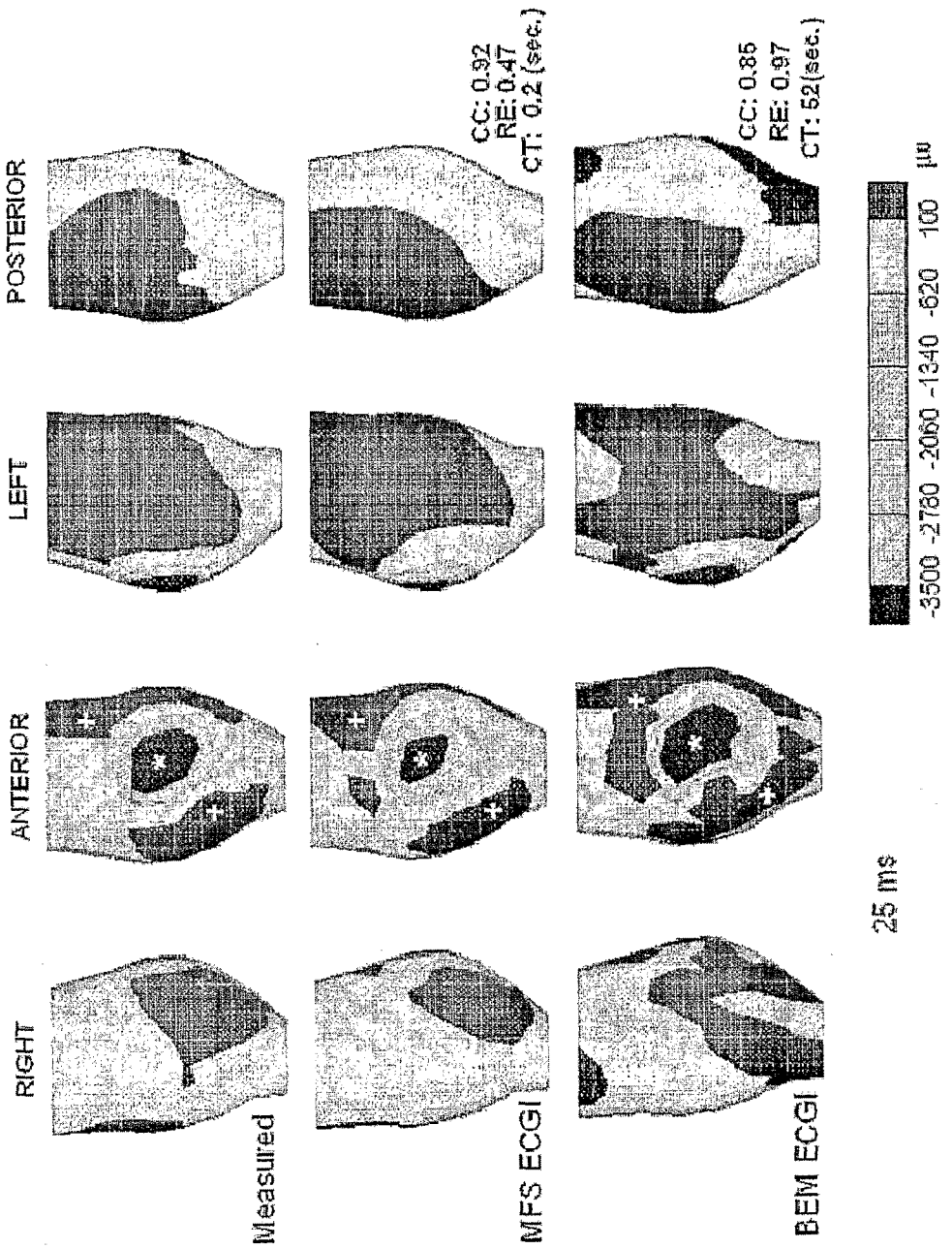
RIGHT
ANTERIOR
LEFT
POSTERIOR
Measured
MFS ECGI
BEM ECGI
CC: 0.92
RE: 0.47
CT: 0.2 (sec.)
CC: 0.85
RE: 0.97
CT: 52(sec.)
25 ms
-3500 -2780 -2060 -1340 -620 100 μV

Figure 9

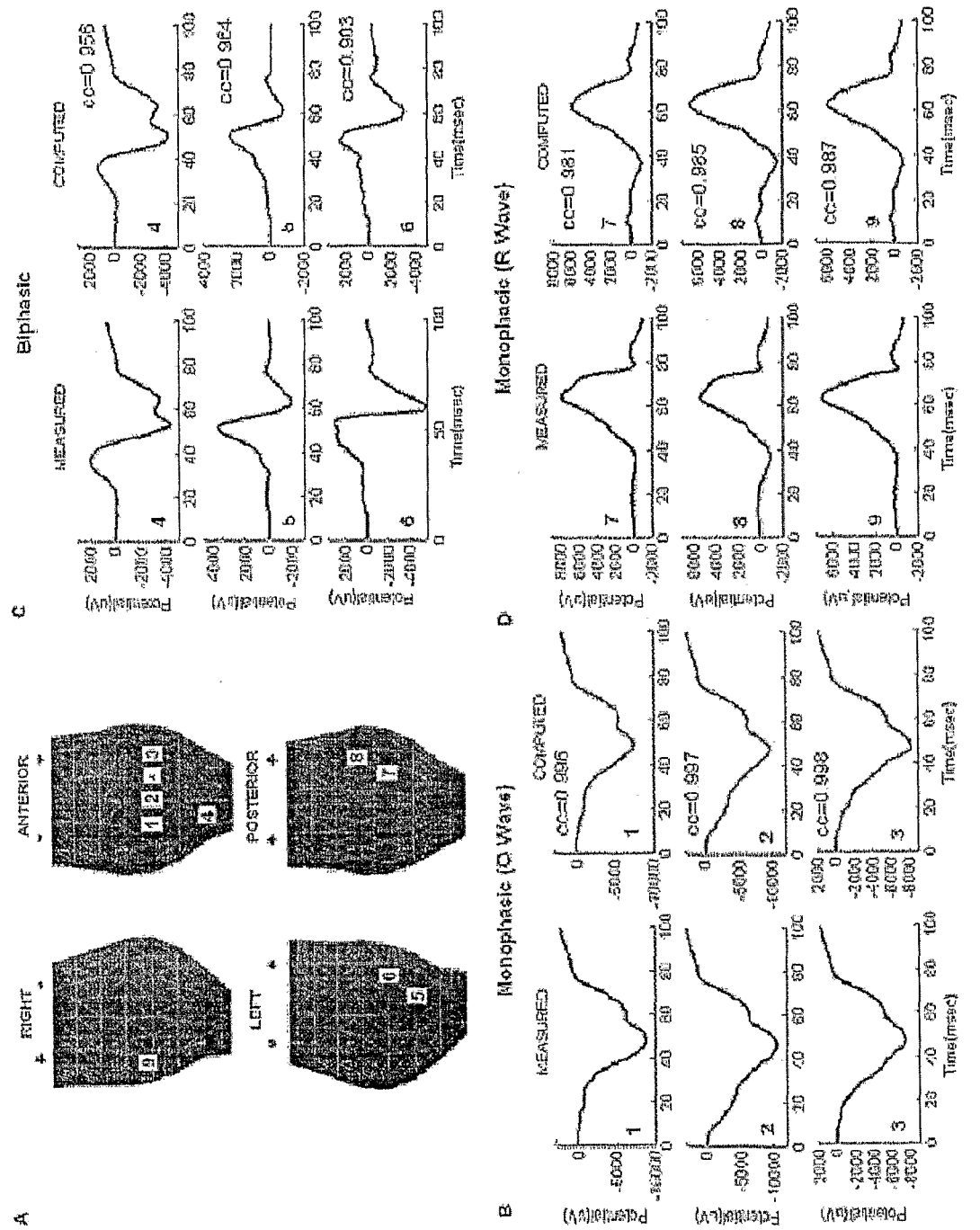
A
RIGHT
ANTERIOR
POSTERIOR
LEFT
B
Monophasic (Q Wave)
MEASURED
COMPUTED
cc=0.996
cc=0.997
cc=0.998
Potential(uV)
Time(msec)
C
Biphasic
MEASURED
COMPUTED
cc=0.956
cc=0.964
cc=0.903
D
Monophasic (R Wave)
MEASURED
COMPUTED
cc=0.981
cc=0.985
cc=0.987

Figure 10

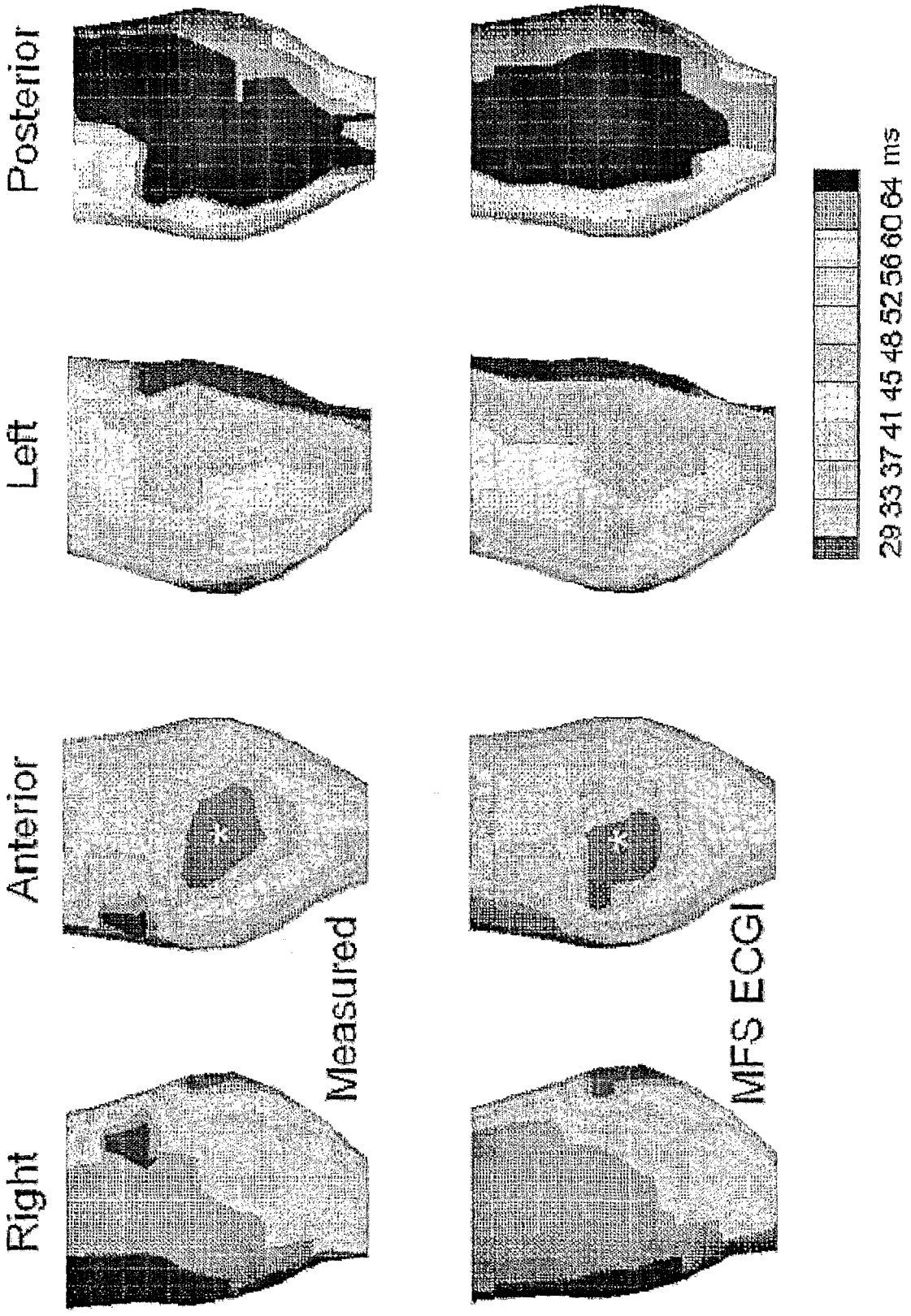
Posterior
Left
Anterior
Right
Measured
MFS ECGI
29 33 37 41 45 48 52 56 60 64 ms

Figure 11

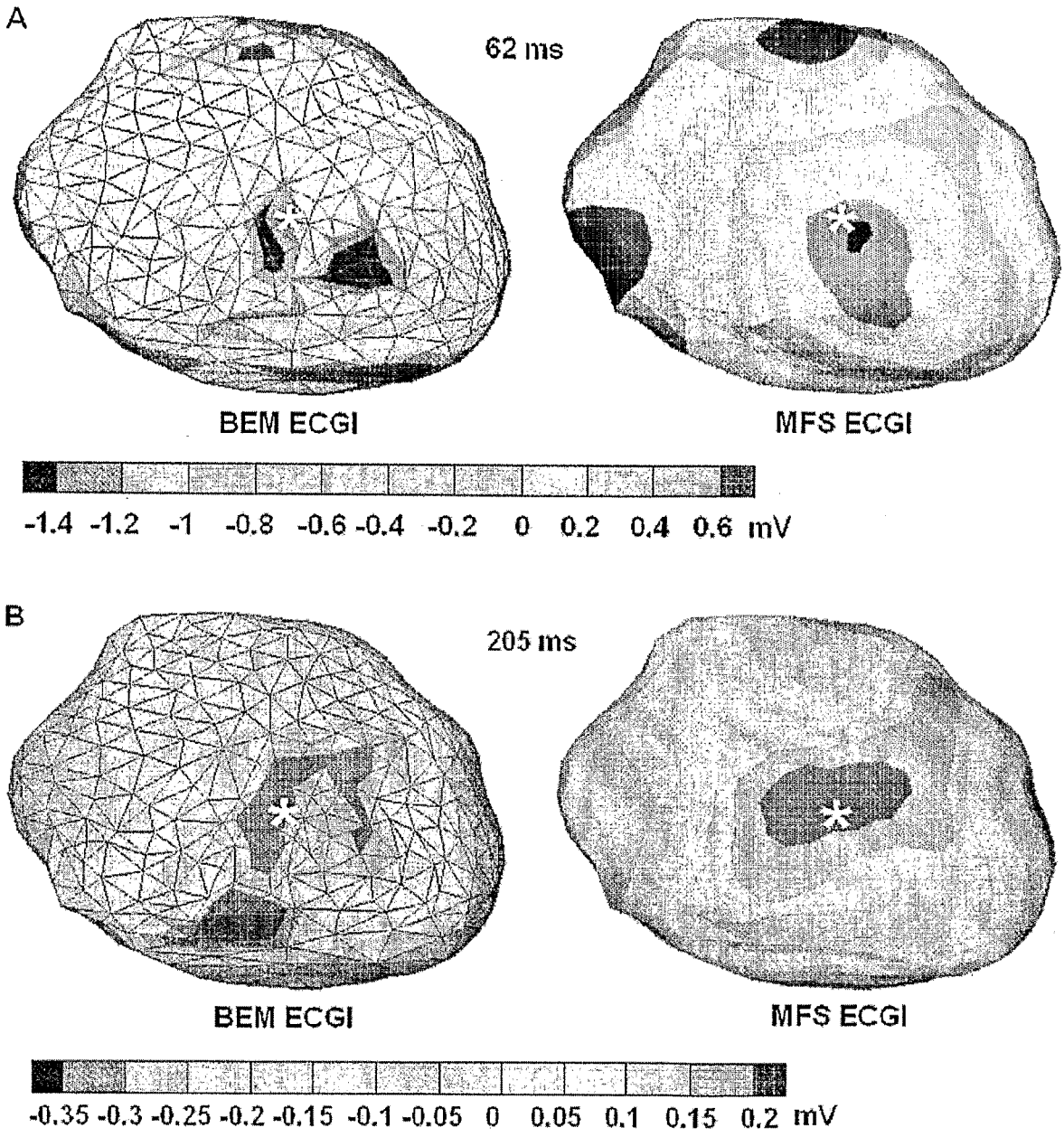
A
62 ms
BEM ECGI
MFS ECGI
-1.4 -1.2 -1 -0.8 -0.6 -0.4 -0.2 0 0.2 0.4 0.6 mV
B
205 ms
BEM ECGI
MFS ECGI
-0.35 -0.3 -0.25 -0.2 -0.15 -0.1 -0.05 0 0.05 0.1 0.15 0.2 mV

Figure 12

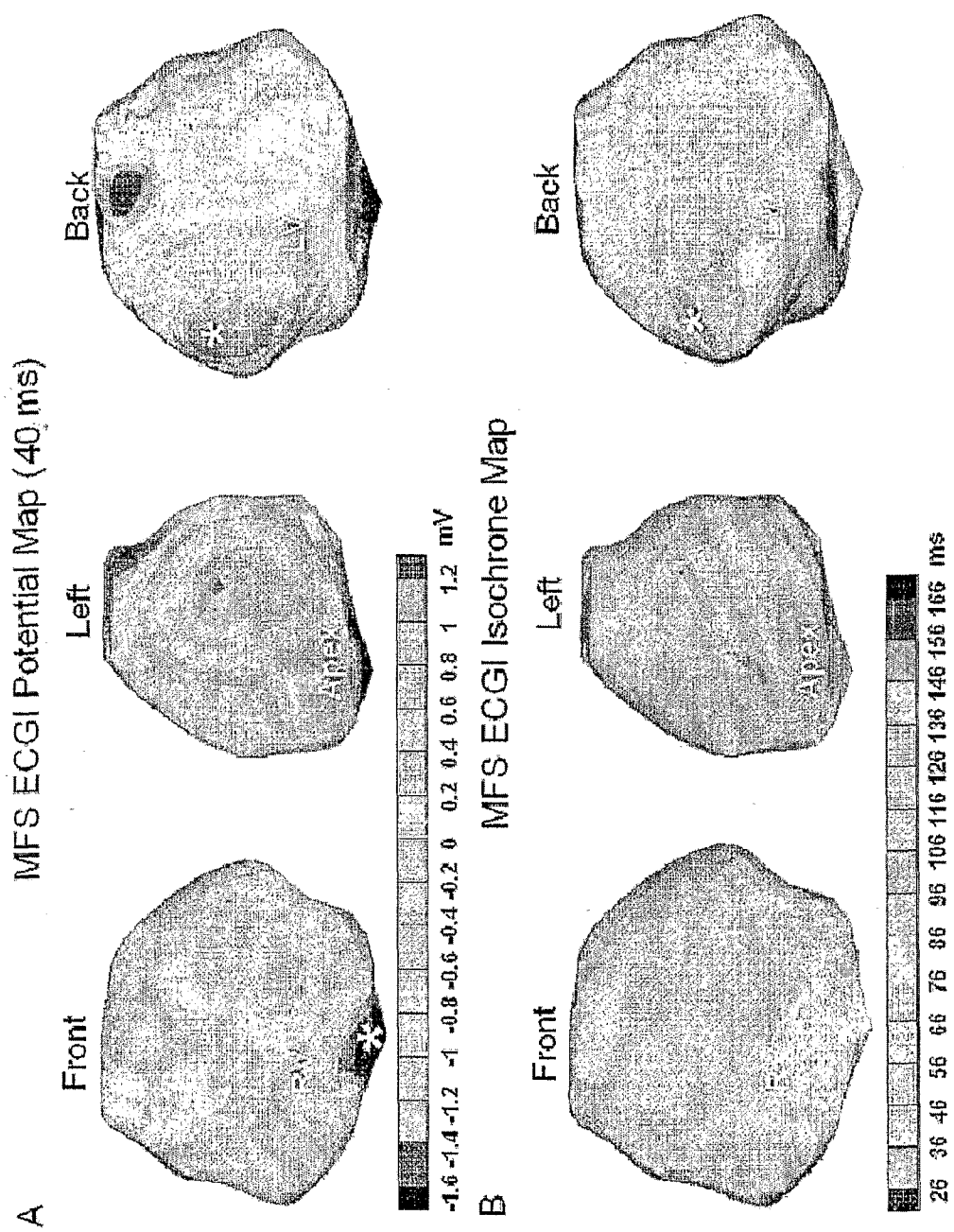
A
MFS ECGI Potential Map (40 ms)
Front
Left
Back
-1.6 -1.4 -1.2 -1 -0.8 -0.6 -0.4 -0.2 0 0.2 0.4 0.6 0.8 1 1.2 mV
B
MFS ECGI Isochrone Map
Front
Left
Back
26 36 46 56 66 76 86 96 106 116 126 136 146 156 166 ms

Figure 13

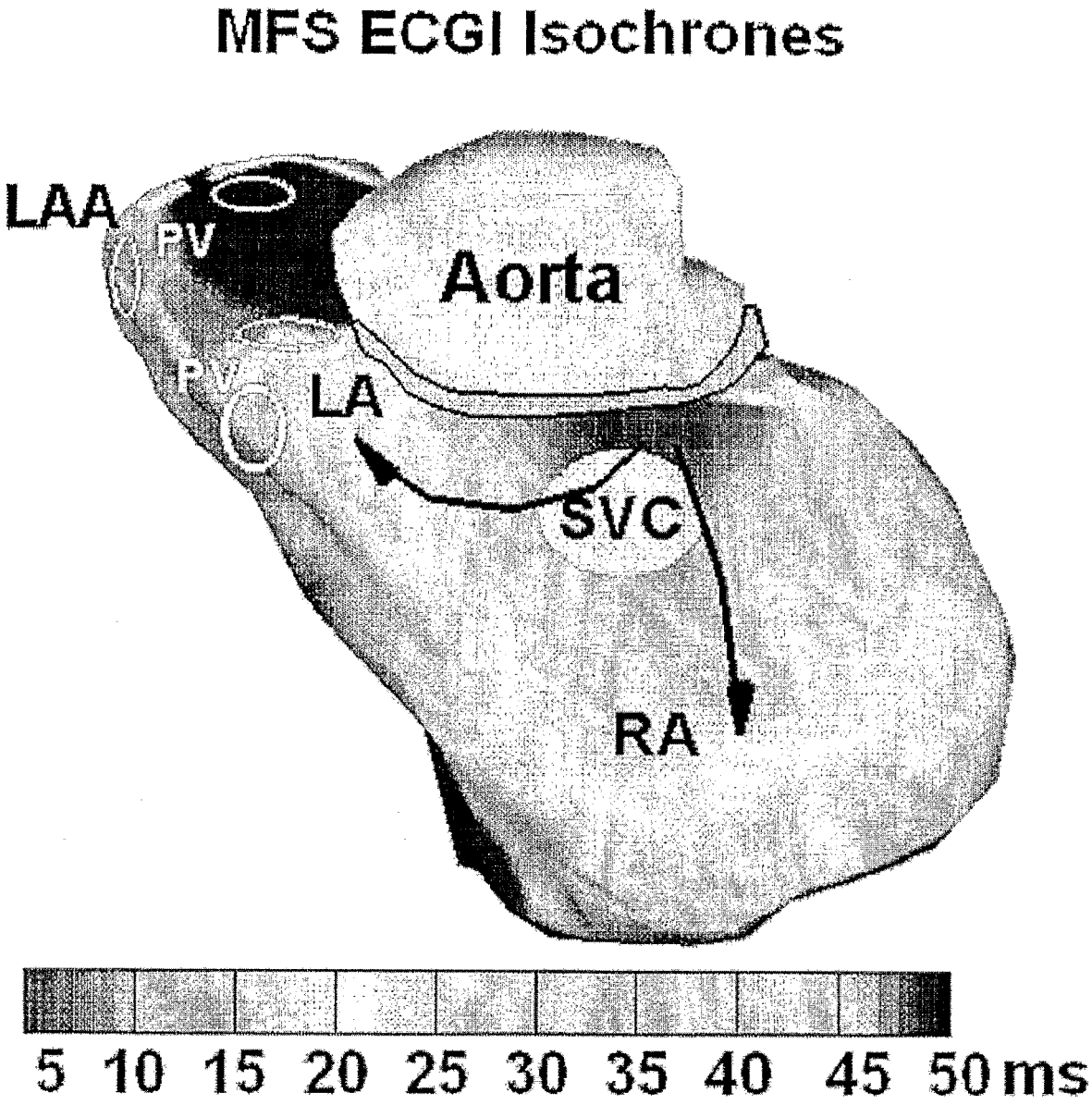
MFS ECGI Isochrones
LAA
PV
PV
Aorta
LA
SVC
RA
5 10 15 20 25 30 35 40 45 50 ms

Figure 14

REFERENCES CITED IN THE DESCRIPTION

This list of references cited by the applicant is for the reader's convenience only. It does not form part of the European patent document. Even though great care has been taken in compiling the references, errors or omissions cannot be excluded and the EPO disclaims all liability in this regard.

Patent documents cited in the description

- US 6772004 B **[0004] [0019] [0022] [0023] [0037] [0040]**
- US 26457202 **[0004]**
- US 20030120163 A **[0004]**
- US 31795302 **[0004]**
- US 20040082870 A **[0004]**
- US 264572 **[0019] [0022] [0023] [0037]**
- US 10317953 B **[0023]**

Non-patent literature cited in the description

- **FISCHER.** *Computer Methods and Programs in Biomedicine,* 1999, vol. 58, 119-131 **[0005]**
- **SEGER.** *Computer Methods and Programs in Biomedicine,* 2005, vol. 77, 242-252 **[0006]**
- **DURRER D. et al.** Total excitation of the isolated human heart. *Circulation,* 1970, vol. 41, 899-91 2 **[0053]**
- **BURNES et al.** A Noninvasive Imaging Modality for Cardiac Arrythmias. *Circulation,* 24 October 2000, 2152-2158 **[0058]**
- **EISENBERG, ANNE.** Beyond the EKG, to a Hypersensitive Heart Monitor. *The New York Times,* 22 April 2004 **[0058]**
- The method of fundamental solutions for problems in potential theory. **FAIRWEATHER ; JOHNSTON.** Treatment of Integral Equations by Numerical Methods. Academic Press, 1982, 349-359 **[0058]**
- **FRIES ; MATTHIES.** Classification and Overview of Meshfree Methods. Institute of Scientific Computing, Technical University Braunschweig, July 2004 **[0058]**
- **GHANEM et al.** Heart-Surface Reconstruction and ECG Electrodes Localization Using Fluoroscopy, Epipolar Geometry and Stereovision: Application to Noninvasive Imaging of Cardiac Electrical Activity. *IEEE Transactions on Medical Imaging,* October 2003, vol. 22 (10), 1307-1318 **[0058]**
- The method of fundamental solutions for diffusion equations. **GOLBERG et al.** Boundary Element Technology XIII **[0058]**
- **WANG ; RUDY.** Application of the Method of Fundamental Solutions to Potential-based Inverse Electrocardiography. *Annals of Biomedical Engineering in or around,* August 2006 **[0058]**
- **Y. C. HON ; T. WEI.** A fundamental solution method for inverse heat conduction problem. *Engineering Analysis with Boundary Elements,* 2004, vol. 28 (5), 489-495 **[0059]**
- **FAIRWEATHER G ; R. L. JOHNSTON.** The method of fundamental solutions for problems in fluid flow. *Appl. Math. Modeling,* 1984, vol. 8, 265-270 **[0059]**
- The method of fundamental solutions for potential, Helmholtz and diffusion problems. **GOLBERG MA ; CHEN CS.** Boundary Integral Methods. Computational Mechanics Publications, 1998, 103-176 **[0059] [0069]**
- **FAIRWEATHER G ; KARAGEORGHIS A.** The method of fundamental solutions for elliptic boundary value problems. *Adv Comput Math,* 1998, vol. 9 (1-2), 69-95 **[0060]**
- **KYTHE PK.** *Fundamental Solutions for Differential Operators and Applications,* 1996 **[0062]**
- The Dual Reciprocity Boundary Element Method. **PATRIDGE, P.W. ; BREBBIA, C.A. ; WROBEL,L.C.** Computational Mechanics Publications. Southampton and Elsevier, 1992 **[0063]**
- **GOLBERG, M.A. ; CHEN, C.S.** Discrete Projection Methods for Integral Equations. Computational Mechanics Publications, 1996 **[0063]**
- **CHEN, Y. ; ATKINSON, K.E.** Solving a Single Layer Integral Equation on Surface in R3. University of Iowa, Department of Mathematics, Technical Report, 1994 **[0063]**
- **KARAGEORGHIS, A. ; FAIRWEATHER, G.** The method of fundamental solutions for the numerical solution of the biharmonic equation. *Journal of Computational Physics,* 1987, vol. 69, 435-459 **[0065]**

专利名称(译)	用于非侵入性心电图图像的系统和方法（ecgd		
公开(公告)号	EP1906821A2	公开(公告)日	2008-04-09
申请号	EP2006800185	申请日	2006-07-21
[标]申请(专利权)人(译)	凯斯西储大学		
申请(专利权)人(译)	凯斯西储大学		
当前申请(专利权)人(译)	凯斯西储大学		
[标]发明人	RUDY YORAM WANG YONG JIA PING		
发明人	RUDY, YORAM WANG, YONG JIA, PING		
IPC分类号	A61B5/04 A61B5/0402 A61B5/00 A61B5/0408 A61B5/055 A61B6/03		
CPC分类号	A61B5/0044 A61B5/0402 A61B5/04085 A61B5/055 A61B6/03		
优先权	60/701626 2005-07-22 US		
其他公开文献	EP1906821A4 EP1906821B1		
外部链接	Espacenet		

摘要(译)

提供了用于确定生物心脏的电活动的非侵入性系统和方法。 处理器被配置为从一组非侵入式测量的体表电势中无网格地计算代表心脏电活动的数据。 使用描述与身体表面电势的测量位置相对应的多个位置与心脏之间的几何关系的数据来实现这一点。